Distribution, Mixing, and Transformation of a Loop Current Ring Waters: The Case of Gulf of Mexico

Mathieu Gentil[1], Enric Pallàs-Sanz[2], Leo Middleton[3], Angel Ruiz-Angulo[4], Thomas Meunier[3], Giovanni Durante[2], Miguel Tenreiro[5], Sheila Natali Estrada-Allis[2], and Julio Sheinbaum Pardo[6]

[1]Centro de Investigación Científica y de Educación Superior de Ensenada, Baja California
[2]Centro de Investigación Científica y de Educación Superior de Ensenada (CICESE)
[3]Woods Hole Oceanographic Institution
[4]University of Iceland
[5]CICESE
[6]Center for Scientific Research and Higher Education at Ensenada

July 11, 2024

Abstract

Mesoscale warm-core rings, known as Loop Current rings (LCRs) reshape the Gulf of Mexico water masses by redistributing large amounts of heat and salt laterally. LCRs also transform water masses via diapycnal mixing, but the mechanisms by which this occurs are poorly measured. Here, we present glider-MicroPod turbulence observations that reveal enhanced mixing below the mixed layer, along the eddy edges, driving the LCR's heat, salt, and oxygen exchanges. Submesoscale stirring at the LCR's edge yields interleavings of adjacent water masses, which facilitates double-diffusive mixing that transforms Subtropical Underwater into Gulf Common Water. Our findings highlight the need for ocean models to parameterize double-diffusive mixing processes directly resulting from submesoscale tracer stirring, which may be important at basin scale in the presence of LCRs in the Gulf of Mexico.

Distribution, Mixing, and Transformation of a Loop Current Ring Waters: The Case of Gulf of Mexico

Mathieu Gentil[1], Enric Pallàs-Sanz[1], Leo Middleton[2], Angel Ruiz-Angulo[3], Thomas Meunier[1,2,4], Giovanni Durante[1], Miguel Tenreiro[1], Sheila N. Allis Estrada[1], Julio Sheinbaum[1]

[1]Center for Scientific Research and Higher Education at Ensenada, Ensenada, Mexico
[2]Woods Hole Oceanographic Institution, Woods Hole, MA, USA
[3]Institute of Earth Sciences, University of Iceland, 102 Reykjavik, Iceland
[4]Laboratoire d'Océanographie Physique et Spatiale (LOPS), University of Brest, CNRS, IRD, Ifremer, IUEM, France

Key Points:

- Direct observations of turbulence reveal the distribution of mixing across a Gulf of Mexico Loop Current Ring.
- Subtropical Underwater is transformed into Gulf Common Water through double-diffusive convection on the edges of the eddy.
- Enhanced submesoscale stirring of spice along the eddy edge leads to double-diffusive convection favorable conditions.

Corresponding author: M. Gentil, m.q.gentil@gmail.com

Abstract

Mesoscale warm-core rings, known as Loop Current rings (LCRs) reshape the Gulf of Mexico water masses by redistributing large amounts of heat and salt laterally. LCRs also transform water masses via diapycnal mixing, but the mechanisms by which this occurs are poorly measured. Here, we present glider-MicroPod turbulence observations that reveal enhanced mixing below the mixed layer, along the eddy edges, driving the LCR's heat, salt, and oxygen exchanges. Submesoscale stirring at the LCR's edge yields interleavings of adjacent water masses, which facilitates double-diffusive mixing that transforms Subtropical Underwater into Gulf Common Water. Our findings highlight the need for ocean models to parameterize double-diffusive mixing processes directly resulting from submesoscale tracer stirring, which may be important at basin scale in the presence of LCRs in the Gulf of Mexico.

Plain Language Summary

In the Gulf of Mexico (GoM), anticyclonic eddies, known as Loop Current rings (LCRs) carrying warm and salty water shape the basin's water mass properties, which in turn, affects the regional climate and marine life. The water mass properties are altered by turbulent mixing. However, the mechanisms leading to the mixing of GoM waters are still under debate due to a lack of observations. Here, we use an autonomous underwater vehicle (glider) equipped with a turbulence sensor to assess the nature of LCR mixing and its impact on water properties. The breaking of internal waves in the ocean is often thought to be responsible for turbulent mixing in the ocean interior. However, our findings demonstrate that a process called double-diffusive convection is responsible, where turbulence is forced by differences between the temperature and salinity of adjacent water parcels. We found that double-diffusive convection was the main driver in mixing heat, salt, and oxygen along the eddy edges, producing Gulf Common Water. These findings highlight the need to include double diffusive processes in ocean models for more accurate simulations.

1 Introduction

Loop Current rings (LCRs) are energetic mesoscale anticyclonic eddies, which transport large amounts of warm and salty Subtropical Underwater (SUW) through the Gulf of Mexico (GoM). These waters are characterized by significant thermohaline anomalies, up to $\sim 10^{\circ}$C and more than 1 psu (Meunier et al., 2018). Because of their large heat and salt content, LCRs influence significantly the GoM's watermass properties (Vidal et al., 1994; P. Hamilton et al., 2018; Meunier et al., 2020), hurricane intensification (Shay et al., 2000; Jaimes et al., 2016; John et al., 2023), sea level rise (Thirion et al., 2024), and biogeochemical cycles (Linacre et al., 2019; Damien et al., 2021). Understanding the processes that control the transformation and variability of LCRs water masses is of climatic and biogeochemical relevance.

As they drift westward through the GoM, LCR waters undergo significant transformations due to surface heat fluxes, river discharge, evaporation, precipitation, as well as isopycnal and diapycnal mixing (P. Hamilton et al., 2018). Recent observations indicate that Ekman buoyancy fluxes may be one of the main drivers of LCRs decay, by converting their available potential energy into kinetic energy (Meunier et al., 2024). Kinetic Energy (KE) is then dissipated through the action of wind stress work, instabilities and turbulent mixing (Herring, 2010; Brannigan, 2016; Sosa-Gutiérrez et al., 2020; Pérez et al., 2022; Meunier et al., 2024). Mixing is likely mediated by submesoscale (1-10 km) processes, which have been observed along the edge of LCRs (Molodtsov et al., 2020) but are too small to be observed by altimetry (Meunier et al., 2020).

Ultimately, water mass properties are irreversibly mixed at the dissipation scale ($\sim$ 1cm−1m). However, different turbulent processes (e.g., shear production and double-diffusion) are associated with different vertical turbulent fluxes between water masses (Kunze, 2003). In shear-driven turbulence, some of the input turbulent kinetic energy (TKE) turns into turbulent dissipation, while some acts in breaking the stratification. In this framework, temperature and salinity are assumed to be mixed vertically with the same effective diffusivity as the buoyancy. Below the mixed layer, vertical shear is mainly attributed to geostrophic currents and internal waves (Pollard et al., 1973; Wu et al., 2015; Pallàs-Sanz et al., 2016; Martínez-Marrero et al., 2019; Fernández-Castro et al., 2020). Alternatively, in double-diffusive convection (DDC), potential energy is converted into TKE, which is then dissipated, and temperature and salinity have differing effective diffusivities. Although previously considered primarily a feature of less active regions, such as the Arctic, recent evidences have shown that double-diffusively unstable stratifications can develop due to the interleaving of water masses via stirring of submesoscale structures (Fine et al., 2022; Sanchez-Rios et al., 2024). This argument was extended by Middleton et al. (2021), who suggested that sub-km stirring could result in DDC at the overturning scale. An outstanding question araises as to the role and contribution of DDC to the LCR's water transformation.

Molodtsov et al. (2020) suggested that the interleaved features along the edge of LCRs were intrusions, similar to those found in the Arctic (Bebieva & Timmermans, 2016), whose dynamics are governed by micro-scale molecular diffusion (B. Ruddick & Richards, 2003). However, Meunier et al. (2019) and Shcherbina et al. (2009) argued that layering and thermohaline interleaving may be created by lateral stirring. Vertically-differential lateral stirring of density-compensating temperature and salinity anomaly may induce a direct variance cascade (Meunier et al., 2015), possibly down to the overturning scales where DDC may become important.

Here, we present direct turbulence observations in an early life-stage LCR drifting through the GoM (the most intense phase of eddy energy decay identified by Meunier et al. (2024)). We use data collected from a ship survey as well as glider observations, to quantify the turbulent mechanisms of LCR's water mass transformation and assess their importance in comparison with the finescale parameterization of double-diffusion. We show that Middleton et al. (2021)'s parameterization provides dissipation rates along the eddy's edge that are consistent with our direct observations. The eddy's turbulent structure is presented, and its variability is discussed within the limitations of the data set. DDC is identified as a key contributor to Subtropical Underwater heat and salt content erosion leading to Gulf Common Water (GCW) production, highlighting the importance of accurate parameterization in ocean models to understand the formation of water masses in the Gulf of Mexico.

2 Data and Methods

2.1 Overview of the experiment

As part of the PhytBloomEddy project ("Phytoplankton Blooms in a Loop Current Eddy"), a multi-platform survey was performed to measure physical and biogeochemical properties within, and at the periphery of, a recently detached LCR.

During a seven-day ship survey in November 2022, microstructure profiles were collected using a VMP-6000 (Vertical Microstructure Profiler) to estimate turbulent dissipation rates. Turbulent data collection was limited to the LCR's west side due to equipment loss. Simultaneously, CTD profiles were gathered using a *Sea-Bird SBE 19 plus* probe. Finally, a Seaglider surveyed the northern edge of the LCR (Fig. 1a), capturing data with horizontal and vertical resolutions of 1 km and 1 m, respectively. The glider was equipped with a *Rockland Scientific MicroPod*, an unpumped *Seabird CTD Sail* probe, and an Anderaa-4831F oxygen sensor.

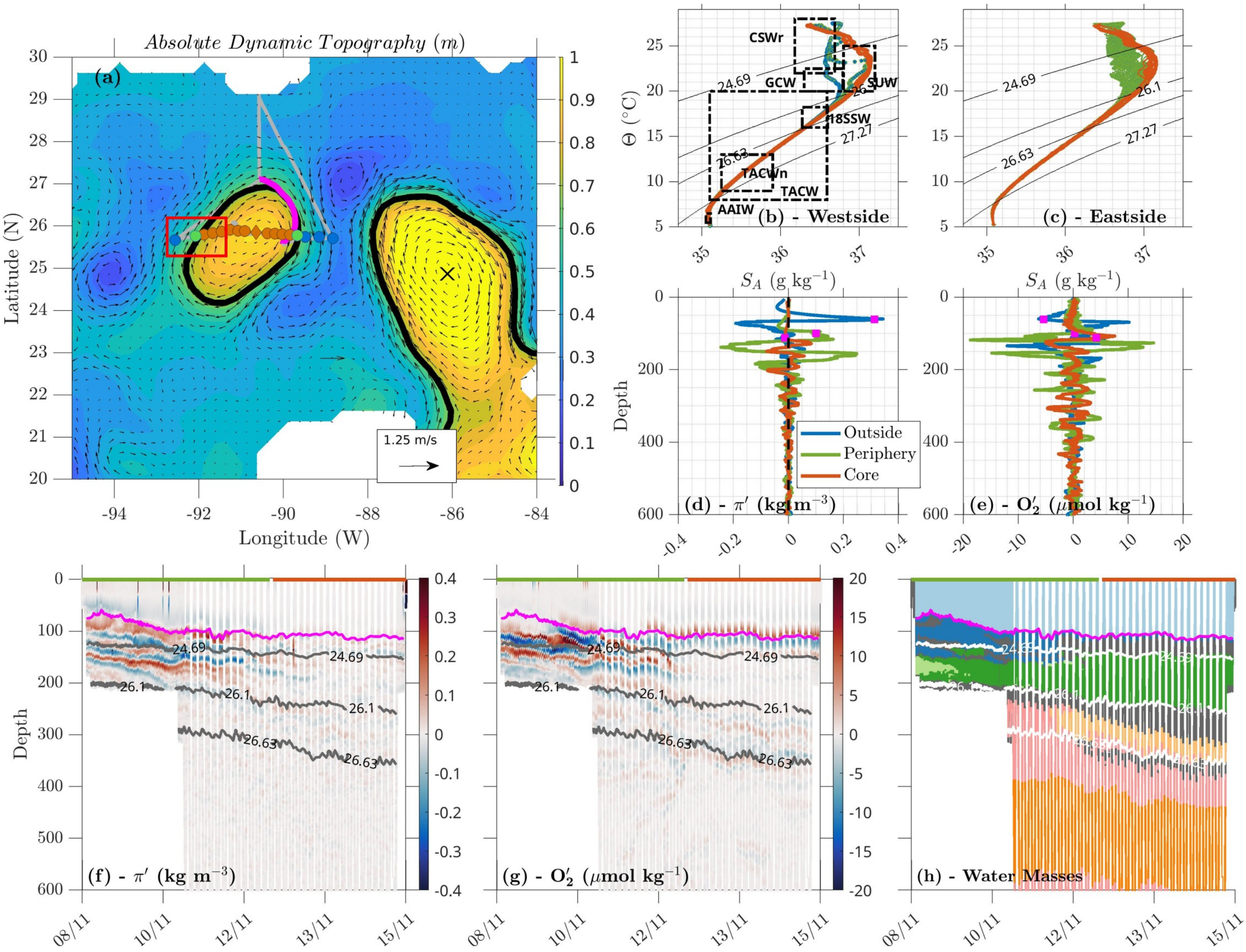

Figure 1. (a) Map of absolute dynamic topography from AVISO averaged between November 7 and 17, 2022. The gray line indicates the ship trajectory, colored circles show CTD stations across the Loop Current Ring (LCR), and red square the vertical microstructure profiler measurements. The black outline indicates the eddy's and Loop Current's contour, and the pink line, the azimuthal Seaglider section. (b) and (c) Conservative temperature - absolute salinity (Θ - S_A) diagrams from R/V Pelican and glider sampling, respectively. Green, blue, and orange dots (lines in d, e, f, g, and h) represent eddy's outside, periphery, and center, respectively. The dashed boxes are Θ - S_A limits of the water masses (colored in (h)), according to the Portela et al. (2018) clasification: CSWr (Caribbean Surface Water remnant - dark blue), GCW (Gulf Common Water - light green), SUW (Subtropical UnderWater - dark green), 18SSW (18°C Sargasso Sea Water - light orange), and TACW (Tropical Atlantic Central Water - pink) and its core (TACWn - dark orange). To complement in (h), light blue and dark gray are the Surface Mixed Layer and the Transtion Layers, respectively. (d, f) spice, (e, g) dissolved oxygen anomalies for eastside (f, g) and westside (d, e) eddy location. Magenta square (d, e) and lines (f, g, h) represent the mixed-layer depth.

Conservative temperature, absolute salinity, potential density anomaly, buoyancy frequency, and spice were computed through the TEOS-10 Gibbs Seawater Oceanographic toolbox (McDougall & Barker, 2011). Spice and dissolved oxygen were high-pass filtered using a second-order Butterworth filter with a cutoff scale of 80 m, following (Meunier et al., 2015). Mean profiles for the LCR and Gulf waters were derived by averaging CTD data (see Figure S1). The LCR's periphery was characterized by wiggling temperature-salinity profiles between GCW and SUW (Fig. 1b). AVISO daily absolute dynamic topography (ADT) was used to detect and track the LCR, following the methodology of Chaigneau et al. (2008) as modified by Sosa-Gutiérrez et al. (2020) (Fig. 1a).

2.2 Microstructure and Turbulence Parameters

Frequent adjustment of the glider's flight along the eddy edge resulted in significant platform vibration. Frajka-Williams et al. (2022), showed that microstructure temperature-based estimates of the dissipation rate, ε, are less contaminated by platform vibration; therefore we focused on the T-S estimates of ε. The temperature-based ε, may be estimated by determining the Batchelor wavenumber, defined by $\kappa_B = (1/2\pi)(\varepsilon/\nu D_T^2)^{1/4}$, and inverting to yield

$$\varepsilon = \nu D_T^2 (2\pi\kappa_B)^4, \tag{1}$$

where ν is the kinematic viscosity of seawater, and D_T=1.44×10^{-7} m^2 s^{-1} is the molecular diffusivity coefficient of temperature. We determined κ_B by fitting a theoretical Batchelor spectrum (Batchelor, 1959) to the observed power spectra of temperature gradients, using the MATLAB toolbox (`https://github.com/bscheife/turbulence_temperature`) (Scheifele et al., 2018), based on the theoretical framework of B. Ruddick et al. (2000) and Peterson and Fer (2014). Power spectrum densities of temperature shear were estimated from 10-s sections of data (with total of 5,120 points), using fast Fourier transform (FFT) on 4-s segments; each spectral point was based on four FFT segments with 50% overlapping.

Assuming a constant eddy diffusivity, κ_z, is estimated from measurements of ε following the Osborn (1980) model :

$$\kappa_z = \Gamma \frac{\varepsilon}{N^2}, \tag{2}$$

where Γ is the mixing coefficient and represents the efficiency of transforming TKE into potential energy and is classically assumed to be 0.2 in the shear-driven regime (Osborn, 1980). Then vertical turbulent heat, salt, and oxygen fluxes, Q_h (W m^{-2}), Q_S (kg m^{-2} s^{-1}), and Q_{O_2} (mmol m^{-2} s^{-1}), respectively, can be computed from κ_z :

$$Qh = -\rho c_p \kappa_z \frac{\partial T}{\partial z}, \tag{3}$$

$$Q_S = \frac{1}{1000}(-\rho\kappa_z \frac{\partial S}{\partial z}), \tag{4}$$

$$Qo_2 = -\kappa_z \frac{\partial [O_2]}{\partial z}, \tag{5}$$

where, ρ is density, c_p is the specific heat capacity of seawater, and $\frac{\partial T}{\partial z}$, $\frac{\partial S}{\partial z}$, $\frac{\partial [O_2]}{\partial z}$ are the vertical shears of potential temperature, absolute salinity and oxygen concentration, respectively. However in DDC (e.g. salt-finger or diffusive-convection), turbulence is driven by the release of potential energy so that the shear-production term of the TKE budget may become negligible and the mixing coefficient can be assumed to be close to

-1 (Laurent & Schmitt, 1999). The subsequent vertical turbulent fluxes of heat and salt may not be estimated with a single constant diffusivity.

To help differentiating DDC from turbulent processes, we used the buoyancy Reynolds number (Gargett, 1988)

$$Re_b = \frac{\epsilon}{\nu N^2}. \tag{6}$$

When Re_b is less than 10, shear-driven turbulence is suppressed by stratification and the resulting buoyancy flux is also suppressed (Stillinger et al., 1983; Shih et al., 2005; Ivey et al., 2008; Bouffard & Boegman, 2013). For large Re_b, the effective turbulent diffusivities for heat and salt become the same (Jackson & Rehmann, 2014). Therefore, we use Re_b to distinguish between DDC and shear-driven turbulence.

Identifying double-diffusive favourable conditions via the density ratio R_ρ is a technique used by many authors (Washburn & Käse, 1987; Schmitt, 1994; Yang et al., 2016; Oyabu et al., 2023), however, the scale at which R_ρ should be measured to infer instability is an important factor. Middleton et al. (2021) suggested that the overturning scale is the relevant scale at which the density ratio must be double-diffusively favourable to force instability, which is usually significantly smaller than the resolution used to calculate R_ρ. They argue that the stirring of compensated thermohaline variance (spice) along isopycnals can lead to double-diffusively favourable R_ρ values on sub-measurement scales. Using this argument, they developed a parameterization for double-diffusive buoyancy fluxes as the result of the stirring motions. The computation of ϵ from this method is detailed in supplementary material, and applied to the glider section. We include the possibility that a background doubly-stable stratification may still support double-diffusive convection due to lateral stirring by using only the buoyancy Reynolds number to distinguish between double-diffusive and shear-driven regimes. This is supported by the results of Middleton et al. (2021).

To compute the DDC-induced heat and salt fluxes, we cannot use a single turbulent diffusivity, so we use the methodology of J. M. Hamilton et al. (1989). Assuming the validity of Osborn and Cox (1972) relationship between heat flux and dissipation of thermal variance χ, and the Osborn (1980) relationship between dissipation rate and buoyancy flux $\epsilon = \Gamma\langle w'b'\rangle$, J. M. Hamilton et al. (1989) derived the relationship:

$$\gamma = \frac{\alpha\langle w'T'\rangle}{\beta\langle w'S'\rangle} \approx \frac{\Gamma R_\rho \Sigma^{DDC}}{R_\rho \Sigma^{DDC} - \Gamma(R_\rho - 1)}, \tag{7}$$

where $\langle\rangle$ is the mean operator between isopycnal layers, $R_\rho = \frac{\alpha\frac{\partial T}{\partial z}}{\beta\frac{\partial S}{\partial z}}$ is the density ratio, α and β are the thermal expansion and haline contraction coefficients, respectively. $\Sigma^{DDC} = \frac{\chi N^2}{2\epsilon(\delta\theta/\delta z)}$ is a scaled dissipation ratio defined by J. M. Hamilton et al. (1989), where χ is the rate of destruction of temperature variance (Osborn & Cox, 1972). The turbulent diffusivities of temperature (κ_T) and salinity (κ_S) could then be estimated from the dissipation rate and the above expression for γ,

$$\kappa_T = \frac{\langle w'T'\rangle}{\langle\theta_z\rangle} = \frac{\langle\epsilon\rangle}{g\alpha\Gamma(1-\gamma^{-1})\langle\theta_z\rangle}, \tag{8}$$

$$\kappa_S = \frac{\langle w'S'\rangle}{\langle S_z\rangle} = \frac{\langle\epsilon\rangle}{g\beta\Gamma(\gamma-1)\langle S_z\rangle}, \tag{9}$$

where $\Gamma = -1$, when double-diffusive convection occurs, and $\Gamma = 0.2$ when shear-driven mixing occurs. Note that if shear-driven mixing dominates, at high buoyancy Reynolds number the effective diffusivities of temperature and salinity are equal, so $\gamma = R_\rho$. As both double diffusion and shear-driven turbulence can drive diapycnal mixing (B. R. Ruddick et al., 2010; Fine et al., 2018, 2022), we chose to consider the distribution of ε as a function of the buoyancy Reynolds number and the density ratio to highlights their importance in the mixing.

2.3 Water Mass Definition and Analysis

The mixed layer depth (MLD) was defined based on a change in density of 0.125 kg m^{-3} from a reference depth of 10 m (Monterey & Levitus, 1997). Water masses were characterized according to the criteria of conservative temperature (θ), absolute salinity (S_A), and dissolved oxygen concentration $[O_2]$ as defined by Portela et al. (2018). To assess the transformation of LCR's water, we employed the Optimal Multiparameter analysis (OMP) (Tomczak Jr, 1981; Tomczak & Large, 1989), using θ, S_A, $[O_2]$, and potential vorticity. The latter was computed following Pérez et al. (2022) for glider observations, with noise reduction techniques for vertical derivatives as suggested by Tomczak (1999). For each observation, the OMP analysis attempts to solve a constrained linear system using the method of least-squares fitting to find the mixing coefficients. The mixing coefficients account for the contribution of each source water type to the sample. Water source types are identified as (quasi) continuous trajectories in the parameter space, based on typical T-S diagrams within the LCR's center and outside (see Figure S1). OMP analysis was applied only in the pycnocline waters (i.e., between 8 and ∼28°C) excluding the mixed layer and the plume-influenced waters, since the method requires avoiding sources and sinks.

3 Results

3.1 LCR's Water Masses Distribution

The LCR is evident in the ADT map of Fig. 1a as a circular patch of high ADT, with a radius of ∼150 km centered at 26°N - 91°W. Fig. 1h shows a vertical section of the water mass distribution along the glider trajectory. Caribbean surface water remnants (CSWr) is evident between the surface and the 24.69 kg m^{-3} isopycnal, which represents the boundary between the mixed layer and the SUW salinity maximum. The CSWr thickness exhibits spatial variability, reaching 60 m near the eddy's periphery, transitioning into a thin layer of 20 m within the eddy center (Fig. 1h).

Within the eddy, the SUW core is found between the 24.69 to 26.1 kg m^{-3} isopycnals, (∼130 to 200 m), with a salinity maximum reaching 37.3 g kg^{-1}. This contrasts with the surrounding GCW outside the eddy, where salinity is lower (36.5 g kg^{-1}; Fig. 1b). Between these watermasses, the $\Theta - S_A$ diagram alternates between SUW and GCW. The glider mission focused on the eddy's boundary to capture this complexity in greater details (Fig. 1c). These high-resolution observations reveal distinct layers of spice anomaly (up to 20 m thick), characterized by alternating signs and amplitudes reaching 0.25 kg m^{-3} (Fig. 1f). Remarkably, similar patterns are observed in the distribution of dissolved oxygen anomaly (Fig. 1g), reaching -20 μmol kg^{-1}, closely aligned with the spice anomaly layers, highlighting the strong link between thermohaline properties and oxygen distribution.

For densities larger than 26.1 kg m^{-3} (>220 m), the Θ-S_A diagram do not show distinctive features between Gulf's and LCR's water (Fig. 1b). Along this isopycnal, where Tropical Atlantic Central Water (TACW), 18°C Sargasso Sea Water (18SSW), and a transitional layer interact (Fig. 1h), spice and oxygen anomaly layers with opposite signs are also observed, but 4 to 5 times weaker than those in shallower regions (Fig. 1f, g). These stacks of thermohaline and biogeochemical layers of alternating signs, evident in glider data in the north east of the eddy, are also shown by CTD casts (Fig. 1d, c).

3.2 Diapycnal Mixing: Distribution, Variability and Origin

High-resolution observations in the LCR reveal significant vertical variability in ε, with values ranging from 10^{-12} to 10^{-7} W kg^{-1} (Fig. 2a). Enhanced turbulent mixing is observed within the ML, as expected by wind and wave and convective effects. However, subsurface regions exhibit distinct zones of elevated ε ($O(10^{-9}/10^{-8})$ W kg^{-1}), highlighting active mixing beyond surface influences.

At the eddy's periphery, where SUW, GCW, and CSWr interact, ε is structured into layers of weak ($O(10^{-11})$ W kg^{-1}) and high ($O(10^{-8})$ W kg^{-1}) intensity, directly overlaying the spice and oxygen anomaly layers (Fig. 1f, g). In these layers, temperature and salinity gradients are compensated in terms of their impact on density (see Figure S2), which is typical of water intrusions or layering as described in Meunier et al. (2019). Molodtsov et al. (2020) suggested the layers were double-diffusive, with a layer of double-convection surrounded by salt-fingering favorable environment (Fig. 2h), where mixing is dominated by molecular diffusion as indicated by the magnitude of χ, which is up to an order of magnitude larger than ε (Fig. 2c).

At the eddy's center, beneath the SUW core, where TACW and 18SSW interact, values of ε up to $O(10^{-8})$ W kg^{-1} are found. Along the isopycnal 26.1 kg m^{-3}, both shear and DDC are involved in mixing (Fig. 2h). High-resolution temperature profiles from the glider thermistor reveal indistinct thermohaline staircases (see Figure S2). Previous studies (Guthrie et al., 2017; Shibley & Timmermans, 2019), suggest that shear forces can disrupt the formation of such staircase structures, even in conditions conducive to DDC such as salt-finger regions. In the eddy center, vertical shear of azimuthal velocity is expected to be very weak, yielding little to no stirring, so that internal waves are likely the dominant mechanism of shear driven-mixing, as found in a similar mesoscale structure in the North Atlantic subtropical gyre (Martínez-Marrero et al., 2019; Fernández-Castro et al., 2020). At the eddy's periphery beyond 220 m depth, a mixture of shear- and DDC-driven mixing is also observed. In that region, which is weakly stratified, the shear associated with the eddy's azimuthal velocity could be sufficiently strong to induce mixing (see Figure S2). Additionally, mooring observations fromPallàs-Sanz et al. (2016) and Martínez-Marrero et al. (2019) show that near-inertial waves may propagate from the surface towards the eddy's base causing enhanced interior mixing.

To examine the spatial variability of ε within the LCR, we compared averaged glider observations and VMP profiles from the eddy's northeastern and western flanks, respectively (Fig. 3). Over 80% of VMP-ε estimates fall within the uncertainty range of the glider-ε estimates (Fig. 3b, c), highlighting relatively homogeneous conditions within the LCR's periphery and center. However, the averaged glider-based ε estimates fail to capture VMP-ε maximum due to the high spatio-temporal variability of fine-scale mixing. At the eddy's periphery, enhanced VMP-ε of $O(10^{-9})$ W kg^{-1} is observed where SUW is found around 180 m depth (Fig. 3b). At this depth, spice anomaly layers with opposite signs are observed from CTD casts (Fig. 1d), indicating it might be the same process (layering) observed by the glider (Fig. 2a). The VMP-ε maxima deeper than 200 m at both eddy's periphery and center are associated with high Re_b ($\sim$100) (see Figure S3), indicating shear-driven mixing likely due to internal wave breaking.

3.3 Turbulent Drivers of Water Masses Transformation

The OMP analysis assesses the contributions of LCR's and Gulf's waters in each glider sample, revealing the significance of the LCR's periphery in the water mass transformation (Fig. 2i). Layering consists in a stacking of thin layers of salty SUW alternating with thin layers of GCW. This process, driven by mesoscale azimuthal perturbations, reduces the vertical scale of thermohaline intrusions ($\sim$15-80 m) (Meunier et al., 2019). At these scales, DDC can trigger overturning even at low buoyancy Reynolds numbers (see Figure S3), enhancing the turbulent fluxes (Fig.2d, e, f), and leading to the forma-

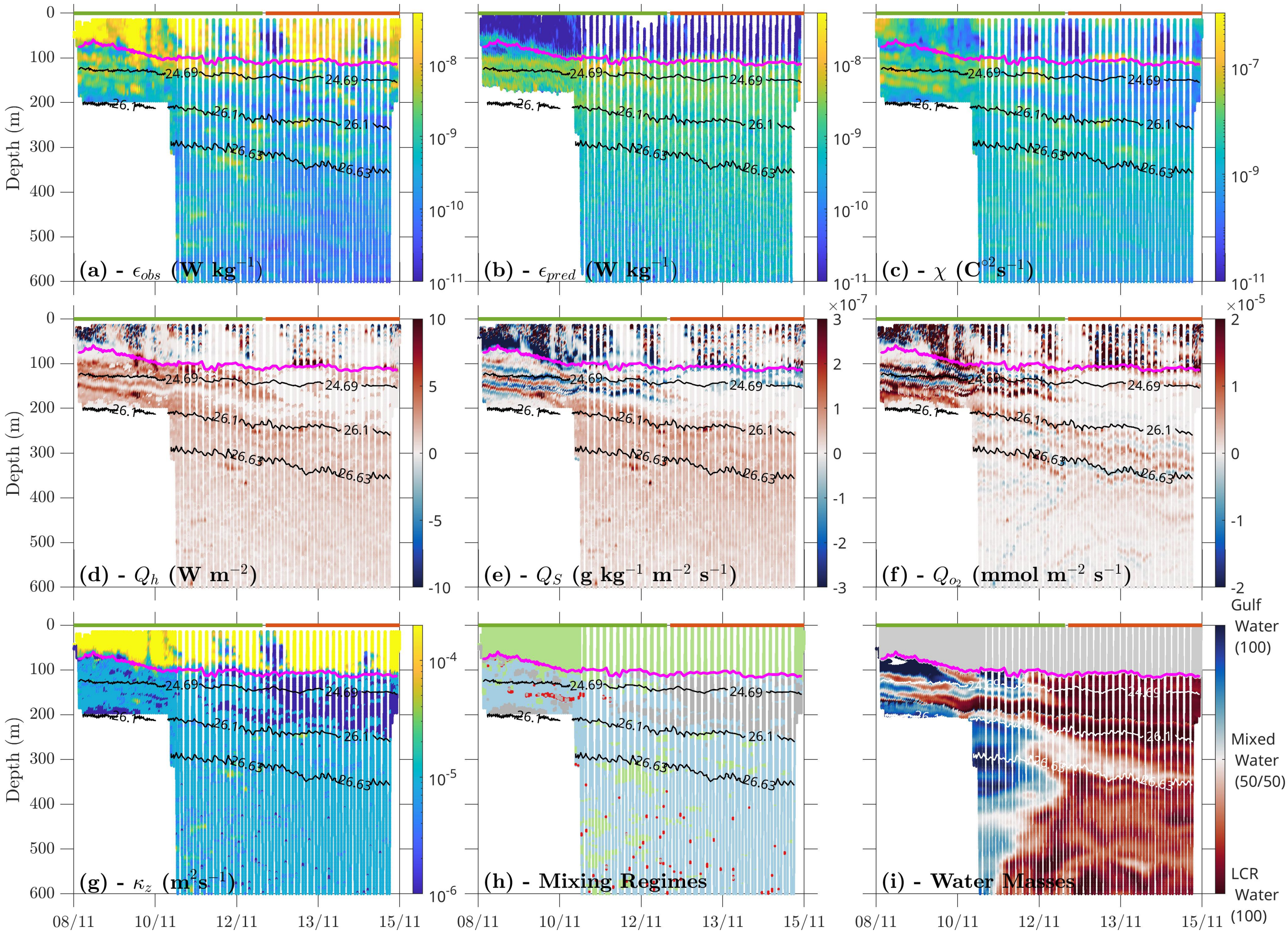

Figure 2. Glider azimuthal section showing: (a) the dissipation rates of turbulent kinetic energy from microstucture; (b) same as (a) but parameterized from Middleton et al. (2021)'s method; (c) the rate of destruction of temperature variance; (d, e, f) vertical turbulent fluxes of heat, salt, and oxygen, respectively; (g) eddy diffusivity; (h) mixing regimes based on the buoyancy Reynolds number and the density ratio, with shear-driven mixing in green, double-convection in red, salt-finger in blue, and areas of no mixing in grey; and (i) water mass transformation expressed as percentages of LCR's and Gulf's waters. The green and orange lines at the top of each panel denote the eddy's periphery and center, respectively. Additionally, the magenta and black lines represent the mixed-layer depth and isopycnes, respectively.

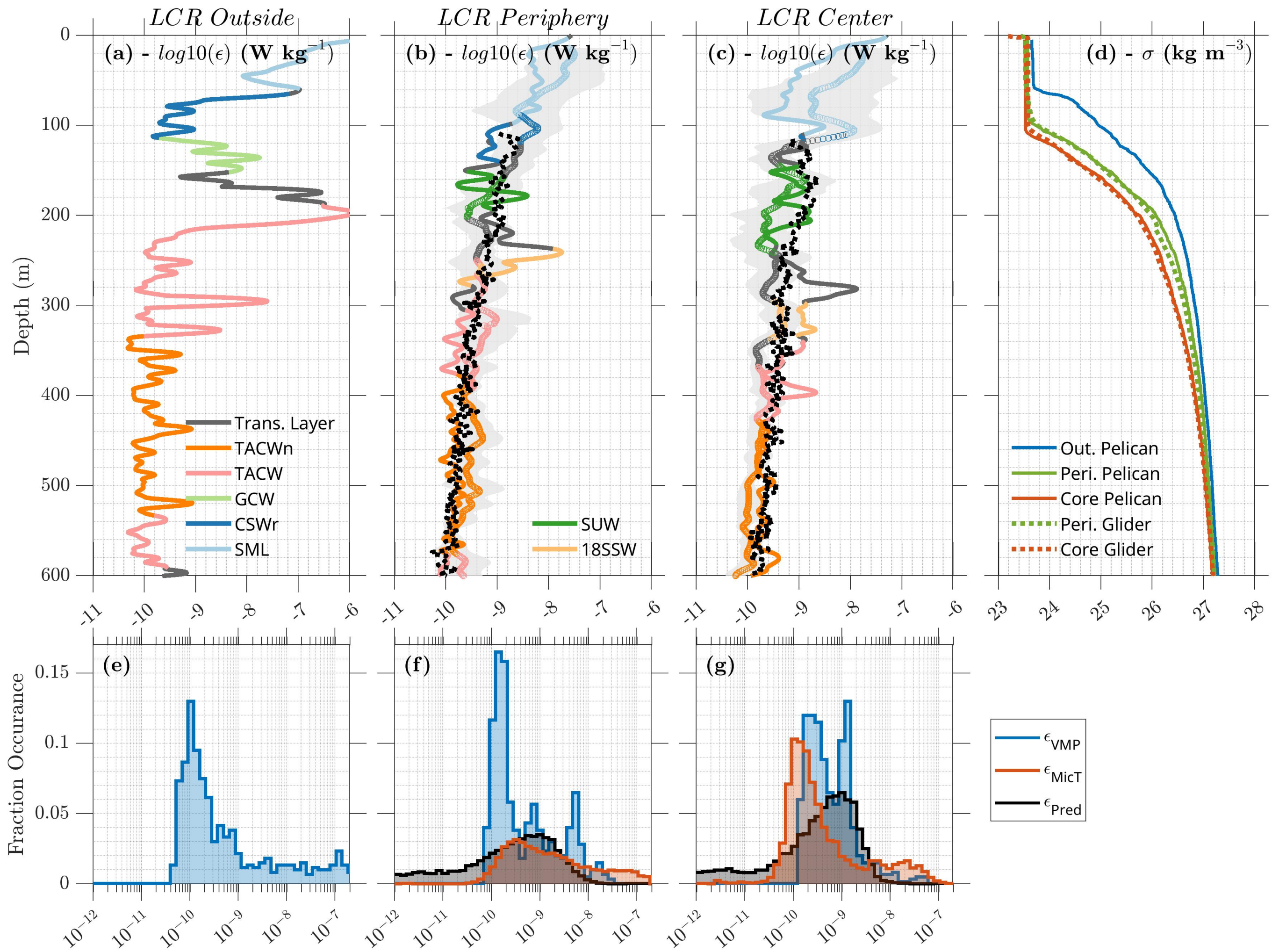

Figure 3. (a, b, c) Averaged profiles of turbulent dissipation rates: solid lines for VMP measurements collected from RV Pelican, colored dots for glider microstructure observations, and black dots for parameterized estimates from double-diffusive convection (Middleton et al., 2021), across eddy periphery and center. Colors correspond to the water masses characterized in Fig. 1h. (d) Profiles of density anomaly sorted by eddy location (Out. for outside, Peri. for periphery) and compared between the different platforms (RV Pelican vs. glider). (e, f, g) Log-histograms comparing predicted dissipation rates (ε_{Pred}) with observed rates from microstructure (ε_{MicT}) and VMP (ε_{VMP}), covering areas outside the eddy (e), its periphery (f), and center (g), respectively.

tion of well-mixed transition layers (Fig.2i). Additional well-mixed regions are observed: (i) between the LCR's periphery and core below 200 m, and (ii) beneath the SUW core in the eddy's center ($\sim$300 m) where oxygen-rich 18SSW water is found (Fig. 1h). Both mixed water columns closely match with increased ε (Fig. 2a), which is induced by a mixture of shear-driven and DDC mixing (Fig. 2h).

Ultimately, watermass properties are irreversibly mixed at the dissipative scale. Fig. 4 illustrates the contribution of different turbulent processes in vertical turbulent fluxes of heat, salt, and oxygen, across the isopycnal layers displayed in Fig. 1b. Vertical fluxes are normalized according to the thickness of each isopycnal layer, allowing for comparison between layers. Although DDC conditions are prevalent in 70% of cases (Fig. 2h), shear-driven mixing is the major contributor to dissipation within the LCR, accounting in average for 78% of observed ε (Fig. 4a). Additionally, 85% of this mixing is localized in the eddy's periphery, highlighting its critical role in transforming water masses, as shown in Fig. 2i. While shear-driven mixing dominates in terms of dissipation, DDC accounts in average for $\sim$70% of the vertical turbulent fluxes of heat, salt, and oxygen (Fig. 4), because of its ability to convert potential energy into TKE, e.g. $\Gamma = -1$, indicating that the effective diffusivity is underestimated by $\Gamma = 0.2$.

The ability of DDC to force turbulence at low Re_b can be assessed in the LCR by comparing the magnitudes and patterns of the observed average dissipation rate, to the predicted dissipation rate from double-diffusive convection parameterized following Middleton et al. (2021) (Fig. 3b, c, black dots). Histograms of the estimated and observed dissipation rates from microstructure show similar distribution in the eddy's periphery (Fig. 3f), and well-reproduce the enhanced ε induced by the layering (Fig. 2b). However, in the eddy center, results show that the parameterized dissipation rate due to DDC is overestimated compared to observations (Fig. 3g). The DDC parameterization assumes a k^{-1} slope for the variance spectrum of spice, which is likely an overestimate in this region due to the weak stirring, leading to the overestimation of mixing within the SUW core (Fig. 2b), as in Fine et al. (2022). Whilst the density ratio Fig. 2h is a mixture of doubly stable, salt fingering favourable and diffusive convection favourable, the buoyancy Reynolds number is skewed to the left, i.e.,<10 (see Figure S3), suggesting that in most cases, stratification suppresses shear-production. Vertical fluxes are therefore largely driven by DDC triggering turbulence in the LCR.

3.4 Vertical Turbulent Fluxes

The vertical fluxes of heat, salt, and oxygen between the isopycnals layers, based on the water mass distribution in the LCR are shown in Figure 4. Our analysis reveals that vertical fluxes of heat and oxygen are predominantly downward (positive), except in the deeper region where oxygen fluxes are upward (negative, Fig. 4b, d). Below the 24.69 kg m^{-3} isopycnal, the water column warms and gains oxygen, as indicated by the positive net fluxes (Fig. 4b, d). In contrast, the layer just below the MLD shows the opposite, with cooling (-412 W m^{-1}) and deoxygenation (-7.9$\times$10^{-4} mmol m^{-1} s^{-1}) due to its interaction with surface forcings. Vertical salt fluxes exhibit a more complex pattern with a divergence around the 24.69 to 26.1 kg m^{-3} isopycnal, where thermohaline intrusions are found (Fig. 2a). The layer above has a net upward flux, while the layer below has a net downward flux (Fig. 4c). Thermohaline intrusions lead to a net downward salt flux of -0.06 10^{-6} g kg^{-1} m^{-1} s^{-1}, where the SUW is found. Therefore, this double-diffusive process contributes to the erosion of the subsurface maximum salinity of the SUW.

Meunier et al. (2020) suggests that lateral mixing at sub-mesoscale scale (<25km) is an important process for LCR's heat dispersion. To get an overview of the turbulent fluxes induced by the thermohaline intrusions, we set $K_{DDC}^{sides} = \Gamma\langle\varepsilon\rangle/\langle N^2\rangle$ with $\Gamma = -1$. This forms the basis for computing horizontal diffusivity for heat, $K_{HT} = K_{DDC}^{sides} T_z^2/T_x^2$

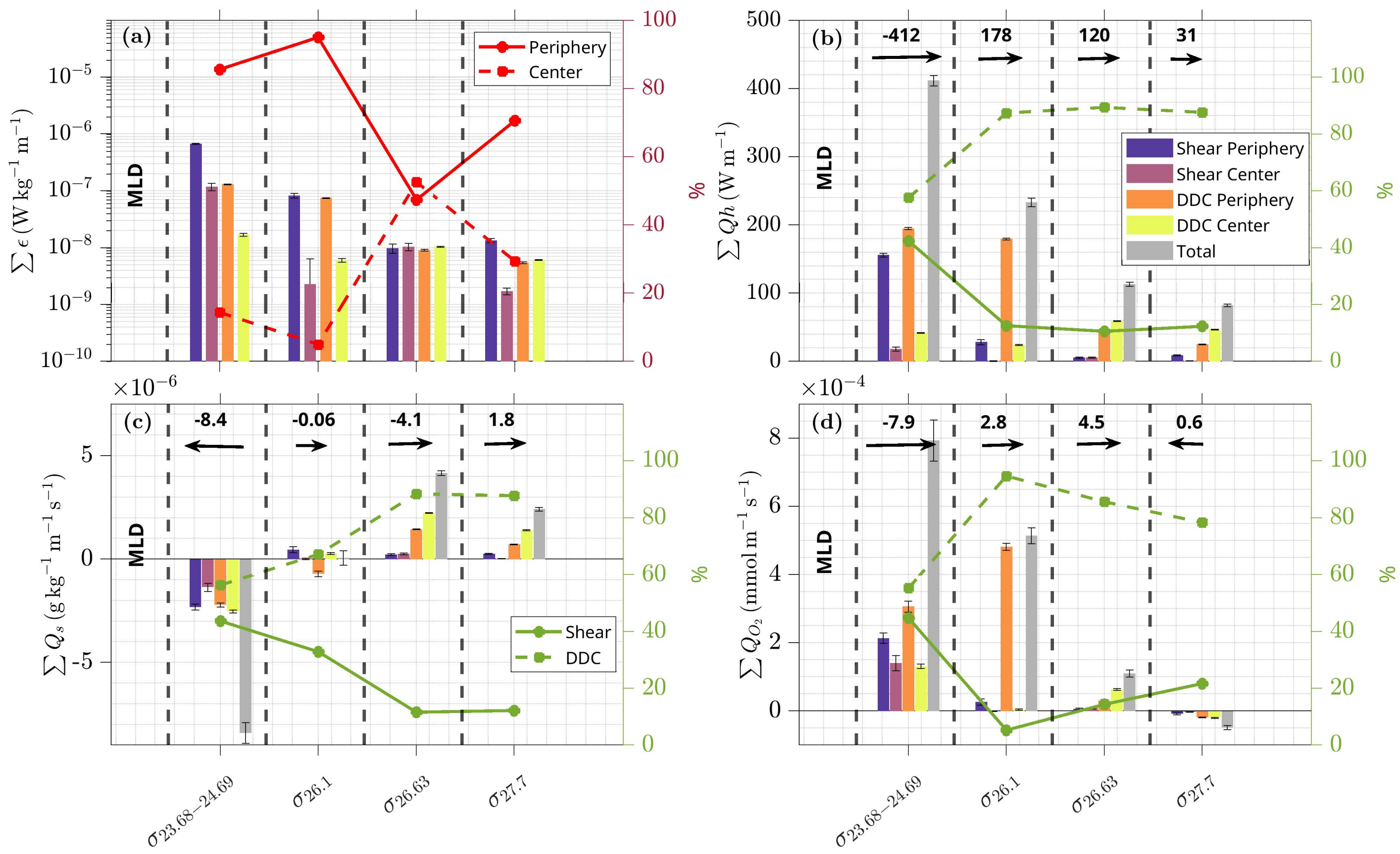

Figure 4. Contribution of (a) dissipation rates and (b, c, d) vertical turbulent fluxes of heat, salt, and oxygen, respectively, segmented by isopycnal layers, based on water mass distribution in the LCR (Fig. 1h). They are categorized by eddy location and mixing nature: shear vs. double-diffusive convection (DDC) (bar color). Relative contributions in each isopycnal layer are shown in % (red and green lines), with net turbulent fluxes changes (+/-) and their directions, downward(upward) fluxes are positive(negative). Vertical fluxes are normalized according to the thickness of each isopycnal layer.

(B. R. Ruddick et al., 2010) and salt, $K_{HS} = K_{DDC}^{sides} S_z^2/S_x^2$ (Hebert et al., 1990). In the thermohaline intrusions, the averaged horizontal heat and salt fluxes are approximately 600 W m^{-2} and 1.8×10^{-5} g kg^{-1} m^{-1} s^{-1}, respectively. These values are two and four orders of magnitude higher than the averaged vertical fluxes, which is consistent with observations in similar finescale structures (Fine et al., 2018; Molodtsov et al., 2020).

4 Summary and Discussion

This observational study provides quantitative estimates of the turbulent processes within an LCR, and their influence on vertical turbulent fluxes and water mass transformation. Our results indicate that shear-driven mixing, does not account for the total heat, salt and oxygen fluxes, and that double-diffusive convection needs to be considered as a key process to explain these turbulent fluxes and water mass transformation.

Through detailed microstructure measurements, we captured the processes driving turbulent mixing. Below the mixed layer, we observed enhanced dissipation rates ($O(10^{-8})$ W kg^{-1}) at the eddy's periphery, beneath its core, and deeper within the eddy. We have shown that DDC can explain the dissipation at the eddy's edges, but not at depth, where it is likely due to internal wave breaking, as observed in various studies (Pallàs-Sanz et al., 2016; Martínez-Marrero et al., 2019; Fernández-Castro et al., 2020). Anticyclonic eddies as LCRs have been shown to induce DDC around their edges in the Arctic (Fine et al., 2018), Mediterranean (Armi et al., 1989; Tokos & Rossby, 1991), Gulf Stream rings (B. R. Ruddick & Bennett, 1985; Schmitt et al., 1986), and the Gulf of Mexico (Meunier et al., 2019; Molodtsov et al., 2020). Additionally, the eddy's periphery emerges as a hotspot responsible for 85% of the total mixing (Fig. 4a), highlighting the need for models to accurately capture this narrow band of few kilometers thick to effectively resolve the processes driving the mesoscale eddy decay.

This study also highlights that submesoscale stirring of spice resulting in DDC is a key mechanism in the route towards transformation of SUW into GCW. We also showed the importance of lateral mixing (few times larger than vertical), associated with thermohaline intrusions, in diffusing the LCR's heat and salt, as suggested in Meunier et al. (2019, 2020). These results challenge the perspective that GCW formation results principally from the vertical mixing of TACW and CSWr (Cervantes-Díaz et al., 2022), suggesting instead that SUW significantly influences GCW formation. Although our observations focus on a single LCR, layering appears to be a recurrent process (Meunier et al., 2019; Molodtsov et al., 2020), and therefore highly relevant for water mass transformation in the GoM.

One important result of this study is the seemingly secondary role played by shear-driven mixing in the eddy's water mass exchanges. Although on average, shear mixing corresponds to $\sim$80% of the total dissipation, the latter accounts for only a third of vertical fluxes within the eddy (Fig. 4). This disparity is attributed to the prevalence of DDC conductive conditions ($\sim$70% of occurrence), where all potential energy is converted into TKE, a mechanism contrasting sharply with shear-driven mixing (Laurent & Schmitt, 1999; Inoue et al., 2007). To verify that DDC is sufficiently strong to control water mass exchanges within the LCR, we applied the parameterization of Middleton et al. (2021) to estimate ε due to double-diffusion. While this method underestimated ε in the high shear regions, it reproduced the enhanced ε observed in the region of enhanced submesoscale stirring on the LCR periphery (Fig. 2b). These findings show that the submesoscale stirring of compensated thermohaline variance (spice) along isopycnals plays an essential role in water mass transformation. Using the classical Osborn (1980) model, with a $\Gamma = 0.2$ suited for shear-driven mixing, leads to a 42% underestimation of vertical turbulent fluxes. However, adjusting $\Gamma = -1$ to capture DDC dynamics (Laurent

& Schmitt, 1999) gives significantly larger rates of vertical turbulent fluxes, hence water mass transformation.

We have shown that double-diffusive convection, favoured by submesoscale stirring, is potentially important in water mass transformation in the Gulf of Mexico. However, the effect of DDC on water mass transformation has not been quantified on a global scale. Given that LCRs are the principal source of water mass variability in the Gulf of Mexico (Portela et al., 2018), an ongoing study is employing both internal-wave (Whalen et al., 2015) and double-diffusive (Middleton et al., 2021) parameterizations to estimate ε across all LCRs identified by the 30 GMOG glider missions since 2016. This effort will aim at enhancing our understanding of warm-core rings' role in tracer transport and diffusion at the basin scale.

5 Open Research

The processed data used in this article needed to understand, evaluate, and build upon the reported research are available in the repository of the Group of Monitoring the Ocean (GMOG). The database is called TurbulentPBE and can accessed using the link `https://gliders.cicese.mx/databases/TurbulentPBE`. Will be required to disclose (i) name, (ii) last name, (iii) e-mail address, (iv) name of the institution, and (v) specify how the TurbulentPBE will be used. GMOG-CICESE will authorize the access and will email to the user a username and password to download the TurbulentPBE database. Anonymous reviewers have granted access to the data, credentials are not required. The TurbulentPBE database can be licensed for non-commerical use, and it is prohibited to share it with third parties, as well as to profit or sell products derived from it. The scripts for microstructure processing are from the MATLAB toolbox (`https://github.com/bscheife/turbulence_temperature`) developed by Scheifele et al. (2018).

Acknowledgments

This work and the postdoctoral fellowship of the corresponding author were supported by the project "Phytoplankton Blooms in a Loop Current Eddy" (FORDECIT-PRONACES/1327709/2020) from Consejo Nacional de Humanidades, Ciencias y Tecnologías de México (CONAHCyT). We acknowledge the contribution of all the staff of Grupo de Monitoreo Oceanográfico con Gliders (GMOG) at the Centro de Investigación Científica y de Educación Superior de Ensenada, Baja California (CICESE), specially to Simo Cusí and Adrian Villicaña for piloting underwater gliders, and to Johanna Saavedra and Eliot Aranda Gonzalez for data management. We are also grateful to the Dr. Anthony Bosse and the Rockland Scientific team, specially the Dr. Anneke ten Doeschate and Evan Cervelli for their support to process glider-MicroPod data.

References

Armi, L., Hebert, D., Oakey, N., Price, J. F., Richardson, P. L., Rossby, H. T., & Ruddick, B. (1989). Two years in the life of a mediterranean salt lens. *Journal of Physical Oceanography*, *19*(3), 354–370.

Batchelor, G. K. (1959). Small-scale variation of convected quantities like temperature in turbulent fluid part 1. general discussion and the case of small conductivity. *Journal of fluid mechanics*, *5*(1), 113–133.

Bebieva, Y., & Timmermans, M.-L. (2016). An examination of double-diffusive processes in a mesoscale eddy in the arctic ocean. *Journal of Geophysical Research: Oceans*, *121*(1), 457–475.

Bouffard, D., & Boegman, L. (2013). A diapycnal diffusivity model for stratified environmental flows. *Dynamics of Atmospheres and Oceans*, *61*, 14–34.

Brannigan, L. (2016). Intense submesoscale upwelling in anticyclonic eddies. *Geo-*

physical Research Letters, *43*(7), 3360–3369.
Cervantes-Díaz, G. Y., Hernández-Ayón, J. M., Zirino, A., Herzka, S. Z., Camacho-Ibar, V., Norzagaray, O., … Delgado, J. A. (2022). Understanding upper water mass dynamics in the gulf of mexico by linking physical and biogeochemical features. *Journal of marine systems*, *225*, 103647.
Chaigneau, A., Gizolme, A., & Grados, C. (2008). Mesoscale eddies off peru in altimeter records: Identification algorithms and eddy spatio-temporal patterns. *Progress in Oceanography*, *79*(2-4), 106–119.
Damien, P., Sheinbaum, J., Pasqueron de Fommervault, O., Jouanno, J., Linacre, L., & Duteil, O. (2021). Do loop current eddies stimulate productivity in the gulf of mexico? *Biogeosciences*, *18*(14), 4281–4303.
Fernández-Castro, B., Evans, D. G., Frajka-Williams, E., Vic, C., & Naveira-Garabato, A. C. (2020). Breaking of internal waves and turbulent dissipation in an anticyclonic mode water eddy. *Journal of Physical Oceanography*, *50*(7), 1893 - 1914. Retrieved from `https://journals.ametsoc.org/view/journals/phoc/50/7/jpoD190168.xml` doi: 10.1175/JPO-D-19-0168.1
Fine, E. C., MacKinnon, J. A., Alford, M. H., & Mickett, J. B. (2018). Microstructure observations of turbulent heat fluxes in a warm-core canada basin eddy. *Journal of Physical Oceanography*, *48*(10), 2397–2418.
Fine, E. C., MacKinnon, J. A., Alford, M. H., Middleton, L., Taylor, J., Mickett, J. B., … Peacock, T. (2022). Double diffusion, shear instabilities, and heat impacts of a pacific summer water intrusion in the beaufort sea. *Journal of Physical Oceanography*, *52*(2), 189–203.
Frajka-Williams, E., Brearley, J. A., Nash, J. D., & Whalen, C. B. (2022). New technological frontiers in ocean mixing. In *Ocean mixing* (pp. 345–361). Elsevier.
Gargett, A. E. (1988). The scaling of turbulence in the presence of stable stratification. *Journal of Geophysical Research: Oceans*, *93*(C5), 5021–5036.
Guthrie, J. D., Fer, I., & Morison, J. H. (2017). Thermohaline staircases in the a mundsen b asin: Possible disruption by shear and mixing. *Journal of Geophysical Research: Oceans*, *122*(10), 7767–7782.
Hamilton, J. M., Lewis, M. R., & Ruddick, B. R. (1989). Vertical fluxes of nitrate associated with salt fingers in the world's oceans. *Journal of Geophysical Research: Oceans*, *94*(C2), 2137–2145.
Hamilton, P., Leben, R., Bower, A., Furey, H., & Pérez-Brunius, P. (2018). Hydrography of the gulf of mexico using autonomous floats. *Journal of Physical Oceanography*, *48*(4), 773–794.
Hebert, D., Oakey, N., & Ruddick, B. (1990). Evolution of a mediterranean salt lens: Scalar properties. *Journal of Physical Oceanography*, *20*(9), 1468–1483.
Herring, H. (2010). *Gulf of mexico hydrographic climatology and method of synthesizing subsurface profiles from the satellite sea surface height anomaly.* Dynalysis of Princeton.
Inoue, R., Yamazaki, H., Wolk, F., Kono, T., & Yoshida, J. (2007). An estimation of buoyancy flux for a mixture of turbulence and double diffusion. *Journal of Physical Oceanography*, *37*(3), 611–624.
Ivey, G., Winters, K., & Koseff, J. (2008). Density stratification, turbulence, but how much mixing? *Annu. Rev. Fluid Mech.*, *40*, 169–184.
Jackson, P. R., & Rehmann, C. R. (2014). Experiments on differential scalar mixing in turbulence in a sheared, stratified flow. *Journal of Physical Oceanography*, *44*(10), 2661–2680.
Jaimes, B., Shay, L. K., & Brewster, J. K. (2016). Observed air-sea interactions in tropical cyclone isaac over loop current mesoscale eddy features. *Dynamics of Atmospheres and Oceans*, *76*, 306–324.
John, E. B., Balaguru, K., Leung, L. R., Foltz, G. R., Hetland, R. D., & Hagos, S. M. (2023). Intensification of hurricane sally (2020) over the mississippi river plume. *Weather and Forecasting*.

Kunze, E. (2003). A review of oceanic salt-fingering theory. *Progress in Oceanography*, *56*(3-4), 399–417.
Laurent, L. S., & Schmitt, R. W. (1999). The contribution of salt fingers to vertical mixing in the north atlantic tracer release experiment. *Journal of Physical Oceanography*, *29*(7), 1404–1424.
Linacre, L., Durazo, R., Camacho-Ibar, V., Selph, K., Lara-Lara, J., Mirabal-Gómez, U., … Sidón-Ceseña, K. (2019). Picoplankton carbon biomass assessments and distribution of prochlorococcus ecotypes linked to loop current eddies during summer in the southern gulf of mexico. *Journal of Geophysical Research: Oceans*, *124*(11), 8342–8359.
Martínez-Marrero, A., Barceló-Llull, B., Pallàs-Sanz, E., Aguiar-González, B., Estrada-Allis, S. N., Gordo, C., … Arístegui, J. (2019). Near-inertial wave trapping near the base of an anticyclonic mesoscale eddy under normal atmospheric conditions. *Journal of Geophysical Research: Oceans*, *124*(11), 8455–8467.
McDougall, T. J., & Barker, P. M. (2011). Getting started with teos-10 and the gibbs seawater (gsw) oceanographic toolbox. *Scor/Iapso WG*, *127*(532), 1–28.
Meunier, T., Bower, A., Pérez-Brunius, P., Graef, F., & Mahadevan, A. (2024). The energy decay of warm-core eddies in the gulf of mexico. *Geophysical Research Letters*, *51*(1), e2023GL106246. Retrieved from `https://agupubs.onlinelibrary.wiley.com/doi/abs/10.1029/2023GL106246` (e2023GL106246 2023GL106246) doi: https://doi.org/10.1029/2023GL106246
Meunier, T., Ménesguen, C., Schopp, R., & Le Gentil, S. (2015). Tracer stirring around a meddy: The formation of layering. *Journal of Physical Oceanography*, *45*(2), 407–423.
Meunier, T., Pallás-Sanz, E., Tenreiro, M., Portela, E., Ochoa, J., Ruiz-Angulo, A., & Cusí, S. (2018). The vertical structure of a loop current eddy. *Journal of Geophysical Research: Oceans*, *123*(9), 6070–6090.
Meunier, T., Sanz, E. P., Tenreiro, M., Ochoa, J., Angulo, A. R., & Buckingham, C. (2019). Observations of layering under a warm-core ring in the gulf of mexico. *Journal of Physical Oceanography*, *49*(12), 3145–3162.
Meunier, T., Sheinbaum, J., Pallàs-Sanz, E., Tenreiro, M., Ochoa, J., Ruiz-Angulo, A., … de Marez, C. (2020). Heat content anomaly and decay of warm-core rings: The case of the gulf of mexico. *Geophysical Research Letters*, *47*(3), e2019GL085600.
Middleton, L., Fine, E., MacKinnon, J., Alford, M., & Taylor, J. (2021). Estimating dissipation rates associated with double diffusion. *Geophysical Research Letters*, *48*(15), e2021GL092779.
Molodtsov, S., Anis, A., Amon, R., & Perez-Brunius, P. (2020). Turbulent mixing in a loop current eddy from glider-based microstructure observations. *Geophysical Research Letters*, *47*(14), e2020GL088033.
Monterey, G. I., & Levitus, S. (1997). Seasonal variability of mixed layer depth for the world ocean.
Osborn, T. R. (1980). Estimates of the local rate of vertical diffusion from dissipation measurements. *Journal of physical oceanography*, *10*(1), 83–89.
Osborn, T. R., & Cox, C. S. (1972). Oceanic fine structure. *Geophysical Fluid Dynamics*, *3*(4), 321–345.
Oyabu, R., Yasuda, I., & Sasaki, Y. (2023). Large-scale distribution and variations of active salt-finger double-diffusion in the western north pacific. *Journal of Physical Oceanography*, *53*(8), 2013–2027.
Pallàs-Sanz, E., Candela, J., Sheinbaum, J., & Ochoa, J. (2016). Mooring observations of the near-inertial wave wake of hurricane ida (2009). *Dynamics of Atmospheres and Oceans*, *76*, 325–344.
Pérez, J., Pallàs-Sanz, E., Tenreiro, M., Meunier, T., Jouanno, J., & Ruiz-Angulo, A. (2022). Overturning instabilities across a warm core ring from glider obser-

vations. *Journal of Geophysical Research: Oceans*, *127*(4), e2021JC017527.

Peterson, A. K., & Fer, I. (2014). Dissipation measurements using temperature microstructure from an underwater glider. *Methods in Oceanography*, *10*, 44–69.

Pollard, R. T., Rhines, P. B., & Thompson, R. O. (1973). The deepening of the wind-mixed layer. *Geophysical Fluid Dynamics*, *4*(4), 381–404.

Portela, E., Tenreiro, M., Pallàs-Sanz, E., Meunier, T., Ruiz-Angulo, A., Sosa-Gutiérrez, R., & Cusí, S. (2018). Hydrography of the central and western gulf of mexico. *Journal of Geophysical Research: Oceans*, *123*(8), 5134–5149.

Ruddick, B., Anis, A., & Thompson, K. (2000). Maximum likelihood spectral fitting: The batchelor spectrum. *Journal of Atmospheric and Oceanic Technology*, *17*(11), 1541–1555.

Ruddick, B., & Richards, K. (2003). Oceanic thermohaline intrusions: Observations. *Progress in Oceanography*, *56*(3-4), 499–527.

Ruddick, B. R., & Bennett, A. S. (1985). Fine structure and mixing at the edge of a warm core ring. *Journal of Geophysical Research: Oceans*, *90*(C5), 8943–8951.

Ruddick, B. R., Oakey, N. S., & Hebert, D. (2010). Measuring lateral heat flux across a thermohaline front: A model and observational test. *Journal of Marine Research*, *68*(3-4), 523–539.

Sanchez-Rios, A., Shearman, R. K., Lee, C. M., Simmons, H. L., St. Laurent, L., Lucas, A. J., … Jan, S. (2024). Characterization of mixing at the edge of a kuroshio intrusion into the south china sea: analysis of thermal variance diffusivity measurements. *Journal of Physical Oceanography*.

Scheifele, B., Waterman, S., Merckelbach, L., & Carpenter, J. R. (2018). Measuring the dissipation rate of turbulent kinetic energy in strongly stratified, low-energy environments: A case study from the arctic ocean. *Journal of Geophysical Research: Oceans*, *123*(8), 5459–5480.

Schmitt, R. W. (1994). Double diffusion in oceanography. *Annual review of fluid mechanics*, *26*(1), 255–285.

Schmitt, R. W., Lueck, R. G., & Joyce, T. M. (1986). Fine-and microstructure at the edge of a warm-core ring. *Deep Sea Research Part A. Oceanographic Research Papers*, *33*(11-12), 1665–1689.

Shay, L. K., Goni, G. J., & Black, P. G. (2000). Effects of a warm oceanic feature on hurricane opal. *Monthly Weather Review*, *128*(5), 1366–1383.

Shcherbina, A. Y., Gregg, M. C., Alford, M. H., & Harcourt, R. R. (2009). Characterizing thermohaline intrusions in the north pacific subtropical frontal zone. *Journal of Physical Oceanography*, *39*(11), 2735–2756.

Shibley, N., & Timmermans, M.-L. (2019). The formation of double-diffusive layers in a weakly turbulent environment. *Journal of Geophysical Research: Oceans*, *124*(3), 1445–1458.

Shih, L. H., Koseff, J. R., Ivey, G. N., & Ferziger, J. H. (2005). Parameterization of turbulent fluxes and scales using homogeneous sheared stably stratified turbulence simulations. *Journal of Fluid Mechanics*, *525*, 193–214.

Sosa-Gutiérrez, R., Pallàs-Sanz, E., Jouanno, J., Chaigneau, A., Candela, J., & Tenreiro, M. (2020). Erosion of the subsurface salinity maximum of the loop current eddies from glider observations and a numerical model. *Journal of Geophysical Research: Oceans*, *125*(7), e2019JC015397.

Stillinger, D., Helland, K., & Van Atta, C. (1983). Experiments on the transition of homogeneous turbulence to internal waves in a stratified fluid. *Journal of Fluid Mechanics*, *131*, 91–122.

Thirion, G., Birol, F., & Jouanno, J. (2024). Loop current eddies as a possible cause of the rapid sea level rise in the gulf of mexico. *Journal of Geophysical Research: Oceans*, *129*(3), e2023JC019764.

Tokos, K. S., & Rossby, T. (1991). Kinematics and dynamics of a mediterranean salt lens. *Journal of Physical Oceanography*, *21*(6), 879–892.

Tomczak, M. (1999). Some historical, theoretical and applied aspects of quantitative water mass analysis. *Journal of Marine Research*, *57*(2), 275–303.

Tomczak, M., & Large, D. G. (1989). Optimum multiparameter analysis of mixing in the thermocline of the eastern indian ocean. *Journal of Geophysical Research: Oceans*, *94*(C11), 16141–16149.

Tomczak Jr, M. (1981). A multi-parameter extension of temperature/salinity diagram techniques for the analysis of non-isopycnal mixing. *Progress in Oceanography*, *10*(3), 147–171.

Vidal, V. M., Vidal, F. V., Hernández, A. F., Meza, E., & Zambrano, L. (1994). Winter water mass distributions in the western gulf of mexico affected by a colliding anticyclonic ring. *Journal of Oceanography*, *50*, 559–588.

Washburn, L., & Käse, R. H. (1987). Double diffusion and the distribution of the density ratio in the mediterranean waterfront southeast of the azores. *Journal of physical oceanography*, *17*(1), 12–25.

Whalen, C. B., MacKinnon, J. A., Talley, L. D., & Waterhouse, A. F. (2015). Estimating the mean diapycnal mixing using a finescale strain parameterization. *Journal of Physical Oceanography*, *45*(4), 1174–1188.

Wu, L., Rutgersson, A., & Sahlée, E. (2015). Upper-ocean mixing due to surface gravity waves. *Journal of Geophysical Research: Oceans*, *120*(12), 8210–8228.

Yang, Y., Verzicco, R., & Lohse, D. (2016). From convection rolls to finger convection in double-diffusive turbulence. *Proceedings of the National Academy of Sciences*, *113*(1), 69–73.

Distribution, Mixing, and Transformation of a Loop Current Ring Waters: The Case of Gulf of Mexico

Mathieu Gentil[1], Enric Pallàs-Sanz[1], Leo Middleton[2], Angel Ruiz-Angulo[3], Thomas Meunier[1,2,4], Giovanni Durante[1], Miguel Tenreiro[1], Sheila N. Allis Estrada[1], Julio Sheinbaum[1]

[1]Center for Scientific Research and Higher Education at Ensenada, Ensenada, Mexico
[2]Woods Hole Oceanographic Institution, Woods Hole, MA, USA
[3]Institute of Earth Sciences, University of Iceland, 102 Reykjavik, Iceland
[4]Laboratoire d'Océanographie Physique et Spatiale (LOPS), University of Brest, CNRS, IRD, Ifremer, IUEM, France

Key Points:

- Direct observations of turbulence reveal the distribution of mixing across a Gulf of Mexico Loop Current Ring.
- Subtropical Underwater is transformed into Gulf Common Water through double-diffusive convection on the edges of the eddy.
- Enhanced submesoscale stirring of spice along the eddy edge leads to double-diffusive convection favorable conditions.

Corresponding author: M. Gentil, `m.q.gentil@gmail.com`

Abstract

Mesoscale warm-core rings, known as Loop Current rings (LCRs) reshape the Gulf of Mexico water masses by redistributing large amounts of heat and salt laterally. LCRs also transform water masses via diapycnal mixing, but the mechanisms by which this occurs are poorly measured. Here, we present glider-MicroPod turbulence observations that reveal enhanced mixing below the mixed layer, along the eddy edges, driving the LCR's heat, salt, and oxygen exchanges. Submesoscale stirring at the LCR's edge yields interleavings of adjacent water masses, which facilitates double-diffusive mixing that transforms Subtropical Underwater into Gulf Common Water. Our findings highlight the need for ocean models to parameterize double-diffusive mixing processes directly resulting from submesoscale tracer stirring, which may be important at basin scale in the presence of LCRs in the Gulf of Mexico.

Plain Language Summary

In the Gulf of Mexico (GoM), anticyclonic eddies, known as Loop Current rings (LCRs) carrying warm and salty water shape the basin's water mass properties, which in turn, affects the regional climate and marine life. The water mass properties are altered by turbulent mixing. However, the mechanisms leading to the mixing of GoM waters are still under debate due to a lack of observations. Here, we use an autonomous underwater vehicle (glider) equipped with a turbulence sensor to assess the nature of LCR mixing and its impact on water properties. The breaking of internal waves in the ocean is often thought to be responsible for turbulent mixing in the ocean interior. However, our findings demonstrate that a process called double-diffusive convection is responsible, where turbulence is forced by differences between the temperature and salinity of adjacent water parcels. We found that double-diffusive convection was the main driver in mixing heat, salt, and oxygen along the eddy edges, producing Gulf Common Water. These findings highlight the need to include double diffusive processes in ocean models for more accurate simulations.

1 Introduction

Loop Current rings (LCRs) are energetic mesoscale anticyclonic eddies, which transport large amounts of warm and salty Subtropical Underwater (SUW) through the Gulf of Mexico (GoM). These waters are characterized by significant thermohaline anomalies, up to $\sim$10°C and more than 1 psu (Meunier et al., 2018). Because of their large heat and salt content, LCRs influence significantly the GoM's watermass properties (Vidal et al., 1994; P. Hamilton et al., 2018; Meunier et al., 2020), hurricane intensification (Shay et al., 2000; Jaimes et al., 2016; John et al., 2023), sea level rise (Thirion et al., 2024), and biogeochemical cycles (Linacre et al., 2019; Damien et al., 2021). Understanding the processes that control the transformation and variability of LCRs water masses is of climatic and biogeochemical relevance.

As they drift westward through the GoM, LCR waters undergo significant transformations due to surface heat fluxes, river discharge, evaporation, precipitation, as well as isopycnal and diapycnal mixing (P. Hamilton et al., 2018). Recent observations indicate that Ekman buoyancy fluxes may be one of the main drivers of LCRs decay, by converting their available potential energy into kinetic energy (Meunier et al., 2024). Kinetic Energy (KE) is then dissipated through the action of wind stress work, instabilities and turbulent mixing (Herring, 2010; Brannigan, 2016; Sosa-Gutiérrez et al., 2020; Pérez et al., 2022; Meunier et al., 2024). Mixing is likely mediated by submesoscale (1-10 km) processes, which have been observed along the edge of LCRs (Molodtsov et al., 2020) but are too small to be observed by altimetry (Meunier et al., 2020).

Ultimately, water mass properties are irreversibly mixed at the dissipation scale ($\sim$ 1cm$-$1m). However, different turbulent processes (e.g., shear production and double-diffusion) are associated with different vertical turbulent fluxes between water masses (Kunze, 2003). In shear-driven turbulence, some of the input turbulent kinetic energy (TKE) turns into turbulent dissipation, while some acts in breaking the stratification. In this framework, temperature and salinity are assumed to be mixed vertically with the same effective diffusivity as the buoyancy. Below the mixed layer, vertical shear is mainly attributed to geostrophic currents and internal waves (Pollard et al., 1973; Wu et al., 2015; Pallàs-Sanz et al., 2016; Martínez-Marrero et al., 2019; Fernández-Castro et al., 2020). Alternatively, in double-diffusive convection (DDC), potential energy is converted into TKE, which is then dissipated, and temperature and salinity have differing effective diffusivities. Although previously considered primarily a feature of less active regions, such as the Arctic, recent evidences have shown that double-diffusively unstable stratifications can develop due to the interleaving of water masses via stirring of submesoscale structures (Fine et al., 2022; Sanchez-Rios et al., 2024). This argument was extended by Middleton et al. (2021), who suggested that sub-km stirring could result in DDC at the overturning scale. An outstanding question araises as to the role and contribution of DDC to the LCR's water transformation.

Molodtsov et al. (2020) suggested that the interleaved features along the edge of LCRs were intrusions, similar to those found in the Arctic (Bebieva & Timmermans, 2016), whose dynamics are governed by micro-scale molecular diffusion (B. Ruddick & Richards, 2003). However, Meunier et al. (2019) and Shcherbina et al. (2009) argued that layering and thermohaline interleaving may be created by lateral stirring. Vertically-differential lateral stirring of density-compensating temperature and salinity anomaly may induce a direct variance cascade (Meunier et al., 2015), possibly down to the overturning scales where DDC may become important.

Here, we present direct turbulence observations in an early life-stage LCR drifting through the GoM (the most intense phase of eddy energy decay identified by Meunier et al. (2024)). We use data collected from a ship survey as well as glider observations, to quantify the turbulent mechanisms of LCR's water mass transformation and assess their importance in comparison with the finescale parameterization of double-diffusion. We show that Middleton et al. (2021)'s parameterization provides dissipation rates along the eddy's edge that are consistent with our direct observations. The eddy's turbulent structure is presented, and its variability is discussed within the limitations of the data set. DDC is identified as a key contributor to Subtropical Underwater heat and salt content erosion leading to Gulf Common Water (GCW) production, highlighting the importance of accurate parameterization in ocean models to understand the formation of water masses in the Gulf of Mexico.

2 Data and Methods

2.1 Overview of the experiment

As part of the PhytBloomEddy project ("Phytoplankton Blooms in a Loop Current Eddy"), a multi-platform survey was performed to measure physical and biogeochemical properties within, and at the periphery of, a recently detached LCR.

During a seven-day ship survey in November 2022, microstructure profiles were collected using a VMP-6000 (Vertical Microstructure Profiler) to estimate turbulent dissipation rates. Turbulent data collection was limited to the LCR's west side due to equipment loss. Simultaneously, CTD profiles were gathered using a *Sea-Bird SBE 19 plus* probe. Finally, a Seaglider surveyed the northern edge of the LCR (Fig. 1a), capturing data with horizontal and vertical resolutions of 1 km and 1 m, respectively. The glider was equipped with a *Rockland Scientific MicroPod*, an unpumped *Seabird CTD Sail* probe, and an Anderaa-4831F oxygen sensor.

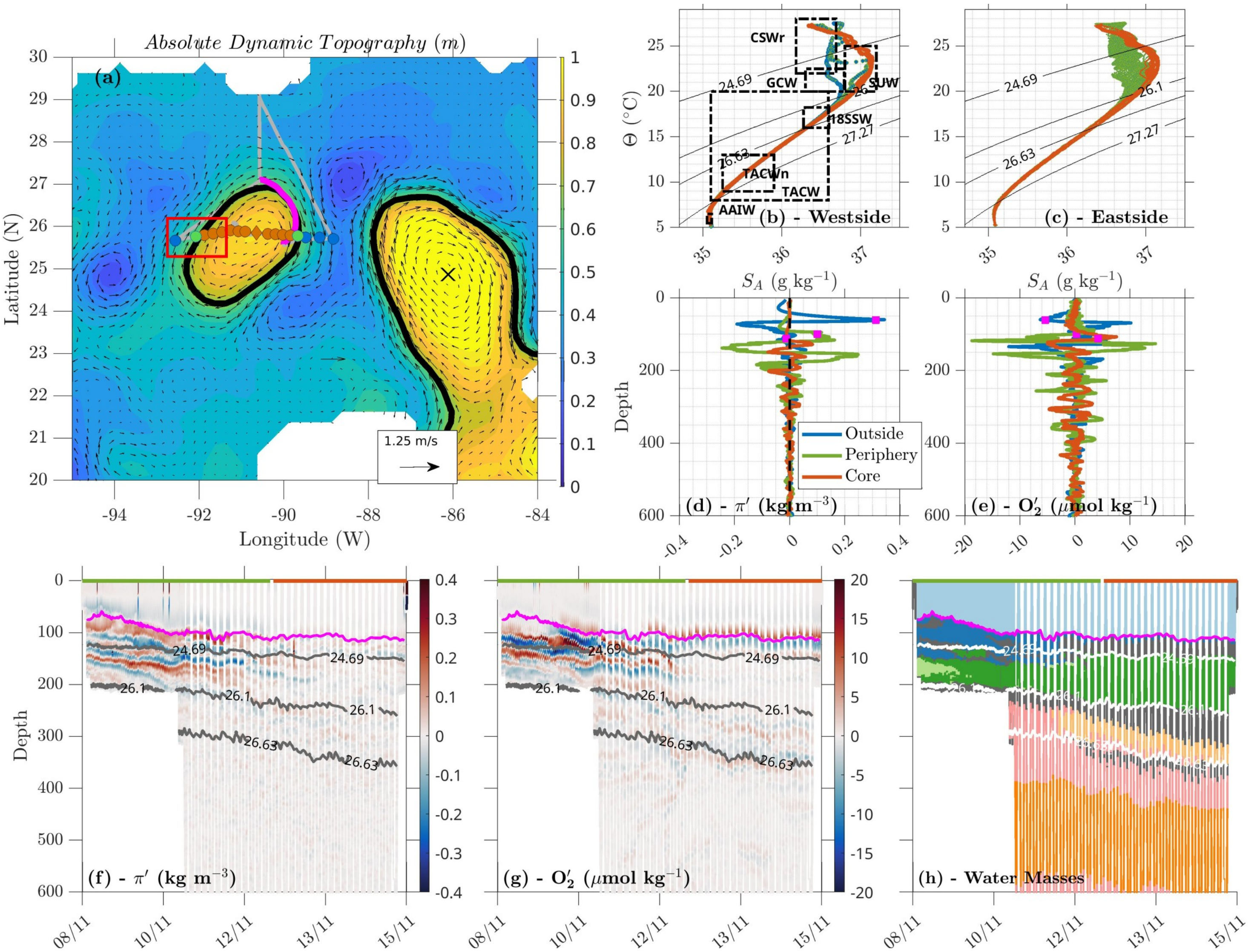

Figure 1. (a) Map of absolute dynamic topography from AVISO averaged between November 7 and 17, 2022. The gray line indicates the ship trajectory, colored circles show CTD stations across the Loop Current Ring (LCR), and red square the vertical microstructure profiler measurements. The black outline indicates the eddy's and Loop Current's contour, and the pink line, the azimuthal Seaglider section. (b) and (c) Conservative temperature - absolute salinity (Θ - S_A) diagrams from R/V Pelican and glider sampling, respectively. Green, blue, and orange dots (lines in d, e, f, g, and h) represent eddy's outside, periphery, and center, respectively. The dashed boxes are Θ - S_A limits of the water masses (colored in (h)), according to the Portela et al. (2018) clasification: CSWr (Caribbean Surface Water remnant - dark blue), GCW (Gulf Common Water - light green), SUW (Subtropical UnderWater - dark green), 18SSW (18°C Sargasso Sea Water - light orange), and TACW (Tropical Atlantic Central Water - pink) and its core (TACWn - dark orange). To complement in (h), light blue and dark gray are the Surface Mixed Layer and the Transtion Layers, respectively. (d, f) spice, (e, g) dissolved oxygen anomalies for eastside (f, g) and westside (d, e) eddy location. Magenta square (d, e) and lines (f, g, h) represent the mixed-layer depth.

Conservative temperature, absolute salinity, potential density anomaly, buoyancy frequency, and spice were computed through the TEOS-10 Gibbs Seawater Oceanographic toolbox (McDougall & Barker, 2011). Spice and dissolved oxygen were high-pass filtered using a second-order Butterworth filter with a cutoff scale of 80 m, following (Meunier et al., 2015). Mean profiles for the LCR and Gulf waters were derived by averaging CTD data (see Figure S1). The LCR's periphery was characterized by wiggling temperature-salinity profiles between GCW and SUW (Fig. 1b). AVISO daily absolute dynamic topography (ADT) was used to detect and track the LCR, following the methodology of Chaigneau et al. (2008) as modified by Sosa-Gutiérrez et al. (2020) (Fig. 1a).

2.2 Microstructure and Turbulence Parameters

Frequent adjustment of the glider's flight along the eddy edge resulted in significant platform vibration. Frajka-Williams et al. (2022), showed that microstructure temperature-based estimates of the dissipation rate, ε, are less contaminated by platform vibration; therefore we focused on the T-S estimates of ε. The temperature-based ε, may be estimated by determining the Batchelor wavenumber, defined by $\kappa_B = (1/2\pi)(\varepsilon/\nu D_T^2)^{1/4}$, and inverting to yield

$$\varepsilon = \nu D_T^2 (2\pi\kappa_B)^4, \tag{1}$$

where ν is the kinematic viscosity of seawater, and D_T=1.44×10^{-7} m^2 s^{-1} is the molecular diffusivity coefficient of temperature. We determined κ_B by fitting a theoretical Batchelor spectrum (Batchelor, 1959) to the observed power spectra of temperature gradients, using the MATLAB toolbox (`https://github.com/bscheife/turbulence_temperature`) (Scheifele et al., 2018), based on the theoretical framework of B. Ruddick et al. (2000) and Peterson and Fer (2014). Power spectrum densities of temperature shear were estimated from 10-s sections of data (with total of 5,120 points), using fast Fourier transform (FFT) on 4-s segments; each spectral point was based on four FFT segments with 50% overlapping.

Assuming a constant eddy diffusivity, κ_z, is estimated from measurements of ε following the Osborn (1980) model :

$$\kappa_z = \Gamma \frac{\varepsilon}{N^2}, \tag{2}$$

where Γ is the mixing coefficient and represents the efficiency of transforming TKE into potential energy and is classically assumed to be 0.2 in the shear-driven regime (Osborn, 1980). Then vertical turbulent heat, salt, and oxygen fluxes, Q_h (W m^{-2}), Q_S (kg m^{-2} s^{-1}), and Q_{O_2} (mmol m^{-2} s^{-1}), respectively, can be computed from κ_z :

$$Qh = -\rho c_p \kappa_z \frac{\partial T}{\partial z}, \tag{3}$$

$$Q_S = \frac{1}{1000}(-\rho\kappa_z \frac{\partial S}{\partial z}), \tag{4}$$

$$Qo_2 = -\kappa_z \frac{\partial [O_2]}{\partial z}, \tag{5}$$

where, ρ is density, c_p is the specific heat capacity of seawater, and $\frac{\partial T}{\partial z}$, $\frac{\partial S}{\partial z}$, $\frac{\partial [O_2]}{\partial z}$ are the vertical shears of potential temperature, absolute salinity and oxygen concentration, respectively. However in DDC (e.g. salt-finger or diffusive-convection), turbulence is driven by the release of potential energy so that the shear-production term of the TKE budget may become negligible and the mixing coefficient can be assumed to be close to

-1 (Laurent & Schmitt, 1999). The subsequent vertical turbulent fluxes of heat and salt may not be estimated with a single constant diffusivity.

To help differentiating DDC from turbulent processes, we used the buoyancy Reynolds number (Gargett, 1988)

$$Re_b = \frac{\epsilon}{\nu N^2}. \tag{6}$$

When Re_b is less than 10, shear-driven turbulence is suppressed by stratification and the resulting buoyancy flux is also suppressed (Stillinger et al., 1983; Shih et al., 2005; Ivey et al., 2008; Bouffard & Boegman, 2013). For large Re_b, the effective turbulent diffusivities for heat and salt become the same (Jackson & Rehmann, 2014). Therefore, we use Re_b to distinguish between DDC and shear-driven turbulence.

Identifying double-diffusive favourable conditions via the density ratio R_ρ is a technique used by many authors (Washburn & Käse, 1987; Schmitt, 1994; Yang et al., 2016; Oyabu et al., 2023), however, the scale at which R_ρ should be measured to infer instability is an important factor. Middleton et al. (2021) suggested that the overturning scale is the relevant scale at which the density ratio must be double-diffusively favourable to force instability, which is usually significantly smaller than the resolution used to calculate R_ρ. They argue that the stirring of compensated thermohaline variance (spice) along isopycnals can lead to double-diffusively favourable R_ρ values on sub-measurement scales. Using this argument, they developed a parameterization for double-diffusive buoyancy fluxes as the result of the stirring motions. The computation of ϵ from this method is detailed in supplementary material, and applied to the glider section. We include the possibility that a background doubly-stable stratification may still support double-diffusive convection due to lateral stirring by using only the buoyancy Reynolds number to distinguish between double-diffusive and shear-driven regimes. This is supported by the results of Middleton et al. (2021).

To compute the DDC-induced heat and salt fluxes, we cannot use a single turbulent diffusivity, so we use the methodology of J. M. Hamilton et al. (1989). Assuming the validity of Osborn and Cox (1972) relationship between heat flux and dissipation of thermal variance χ, and the Osborn (1980) relationship between dissipation rate and buoyancy flux $\epsilon = \Gamma\langle w'b'\rangle$, J. M. Hamilton et al. (1989) derived the relationship:

$$\gamma = \frac{\alpha\langle w'T'\rangle}{\beta\langle w'S'\rangle} \approx \frac{\Gamma R_\rho \Sigma^{DDC}}{R_\rho \Sigma^{DDC} - \Gamma(R_\rho - 1)}, \tag{7}$$

where $\langle\rangle$ is the mean operator between isopycnal layers, $R_\rho = \frac{\alpha\frac{\partial T}{\partial z}}{\beta\frac{\partial S}{\partial z}}$ is the density ratio, α and β are the thermal expansion and haline contraction coefficients, respectively. $\Sigma^{DDC} = \frac{\chi N^2}{2\epsilon(\delta\theta/\delta z)}$ is a scaled dissipation ratio defined by J. M. Hamilton et al. (1989), where χ is the rate of destruction of temperature variance (Osborn & Cox, 1972). The turbulent diffusivities of temperature (κ_T) and salinity (κ_S) could then be estimated from the dissipation rate and the above expression for γ,

$$\kappa_T = \frac{\langle w'T'\rangle}{\langle\theta_z\rangle} = \frac{\langle\epsilon\rangle}{g\alpha\Gamma(1-\gamma^{-1})\langle\theta_z\rangle}, \tag{8}$$

$$\kappa_S = \frac{\langle w'S'\rangle}{\langle S_z\rangle} = \frac{\langle\epsilon\rangle}{g\beta\Gamma(\gamma-1)\langle S_z\rangle}, \tag{9}$$

where $\Gamma = -1$, when double-diffusive convection occurs, and $\Gamma = 0.2$ when shear-driven mixing occurs. Note that if shear-driven mixing dominates, at high buoyancy Reynolds number the effective diffusivities of temperature and salinity are equal, so $\gamma = R_\rho$. As both double diffusion and shear-driven turbulence can drive diapycnal mixing (B. R. Ruddick et al., 2010; Fine et al., 2018, 2022), we chose to consider the distribution of ε as a function of the buoyancy Reynolds number and the density ratio to highlights their importance in the mixing.

2.3 Water Mass Definition and Analysis

The mixed layer depth (MLD) was defined based on a change in density of 0.125 kg m^{-3} from a reference depth of 10 m (Monterey & Levitus, 1997). Water masses were characterized according to the criteria of conservative temperature (θ), absolute salinity (S_A), and dissolved oxygen concentration $[O_2]$ as defined by Portela et al. (2018). To assess the transformation of LCR's water, we employed the Optimal Multiparameter analysis (OMP) (Tomczak Jr, 1981; Tomczak & Large, 1989), using θ, S_A, $[O_2]$, and potential vorticity. The latter was computed following Pérez et al. (2022) for glider observations, with noise reduction techniques for vertical derivatives as suggested by Tomczak (1999). For each observation, the OMP analysis attempts to solve a constrained linear system using the method of least-squares fitting to find the mixing coefficients. The mixing coefficients account for the contribution of each source water type to the sample. Water source types are identified as (quasi) continuous trajectories in the parameter space, based on typical T-S diagrams within the LCR's center and outside (see Figure S1). OMP analysis was applied only in the pycnocline waters (i.e., between 8 and $\sim$28°C) excluding the mixed layer and the plume-influenced waters, since the method requires avoiding sources and sinks.

3 Results

3.1 LCR's Water Masses Distribution

The LCR is evident in the ADT map of Fig. 1a as a circular patch of high ADT, with a radius of $\sim$150 km centered at 26°N - 91°W. Fig. 1h shows a vertical section of the water mass distribution along the glider trajectory. Caribbean surface water remnants (CSWr) is evident between the surface and the 24.69 kg m^{-3} isopycnal, which represents the boundary between the mixed layer and the SUW salinity maximum. The CSWr thickness exhibits spatial variability, reaching 60 m near the eddy's periphery, transitioning into a thin layer of 20 m within the eddy center (Fig. 1h).

Within the eddy, the SUW core is found between the 24.69 to 26.1 kg m^{-3} isopycnals, ($\sim$130 to 200 m), with a salinity maximum reaching 37.3 g kg^{-1}. This contrasts with the surrounding GCW outside the eddy, where salinity is lower (36.5 g kg^{-1}; Fig. 1b). Between these watermasses, the $\Theta - S_A$ diagram alternates between SUW and GCW. The glider mission focused on the eddy's boundary to capture this complexity in greater details (Fig. 1c). These high-resolution observations reveal distinct layers of spice anomaly (up to 20 m thick), characterized by alternating signs and amplitudes reaching 0.25 kg m^{-3} (Fig. 1f). Remarkably, similar patterns are observed in the distribution of dissolved oxygen anomaly (Fig. 1g), reaching -20 μmol kg^{-1}, closely aligned with the spice anomaly layers, highlighting the strong link between thermohaline properties and oxygen distribution.

For densities larger than 26.1 kg m^{-3} (>220 m), the Θ-S_A diagram do not show distinctive features between Gulf's and LCR's water (Fig. 1b). Along this isopycnal, where Tropical Atlantic Central Water (TACW), 18°C Sargasso Sea Water (18SSW), and a transitional layer interact (Fig. 1h), spice and oxygen anomaly layers with opposite signs are also observed, but 4 to 5 times weaker than those in shallower regions (Fig. 1f, g). These stacks of thermohaline and biogeochemical layers of alternating signs, evident in glider data in the north east of the eddy, are also shown by CTD casts (Fig. 1d, c).

3.2 Diapycnal Mixing: Distribution, Variability and Origin

High-resolution observations in the LCR reveal significant vertical variability in ε, with values ranging from 10^{-12} to 10^{-7} W kg^{-1} (Fig. 2a). Enhanced turbulent mixing is observed within the ML, as expected by wind and wave and convective effects. However, subsurface regions exhibit distinct zones of elevated ε ($O(10^{-9}/10^{-8})$ W kg^{-1}), highlighting active mixing beyond surface influences.

At the eddy's periphery, where SUW, GCW, and CSWr interact, ε is structured into layers of weak ($O(10^{-11})$ W kg^{-1}) and high ($O(10^{-8})$ W kg^{-1}) intensity, directly overlaying the spice and oxygen anomaly layers (Fig. 1f, g). In these layers, temperature and salinity gradients are compensated in terms of their impact on density (see Figure S2), which is typical of water intrusions or layering as described in Meunier et al. (2019). Molodtsov et al. (2020) suggested the layers were double-diffusive, with a layer of double-convection surrounded by salt-fingering favorable environment (Fig. 2h), where mixing is dominated by molecular diffusion as indicated by the magnitude of χ, which is up to an order of magnitude larger than ε (Fig. 2c).

At the eddy's center, beneath the SUW core, where TACW and 18SSW interact, values of ε up to $O(10^{-8})$ W kg^{-1} are found. Along the isopycnal 26.1 kg m^{-3}, both shear and DDC are involved in mixing (Fig. 2h). High-resolution temperature profiles from the glider thermistor reveal indistinct thermohaline staircases (see Figure S2). Previous studies (Guthrie et al., 2017; Shibley & Timmermans, 2019), suggest that shear forces can disrupt the formation of such staircase structures, even in conditions conducive to DDC such as salt-finger regions. In the eddy center, vertical shear of azimuthal velocity is expected to be very weak, yielding little to no stirring, so that internal waves are likely the dominant mechanism of shear driven-mixing, as found in a similar mesoscale structure in the North Atlantic subtropical gyre (Martínez-Marrero et al., 2019; Fernández-Castro et al., 2020). At the eddy's periphery beyond 220 m depth, a mixture of shear- and DDC-driven mixing is also observed. In that region, which is weakly stratified, the shear associated with the eddy's azimuthal velocity could be sufficiently strong to induce mixing (see Figure S2). Additionally, mooring observations fromPallàs-Sanz et al. (2016) and Martínez-Marrero et al. (2019) show that near-inertial waves may propagate from the surface towards the eddy's base causing enhanced interior mixing.

To examine the spatial variability of ε within the LCR, we compared averaged glider observations and VMP profiles from the eddy's northeastern and western flanks, respectively (Fig. 3). Over 80% of VMP-ε estimates fall within the uncertainty range of the glider-ε estimates (Fig. 3b, c), highlighting relatively homogeneous conditions within the LCR's periphery and center. However, the averaged glider-based ε estimates fail to capture VMP-ε maximum due to the high spatio-temporal variability of fine-scale mixing. At the eddy's periphery, enhanced VMP-ε of $O(10^{-9})$ W kg^{-1} is observed where SUW is found around 180 m depth (Fig. 3b). At this depth, spice anomaly layers with opposite signs are observed from CTD casts (Fig. 1d), indicating it might be the same process (layering) observed by the glider (Fig. 2a). The VMP-ε maxima deeper than 200 m at both eddy's periphery and center are associated with high Re_b ($\sim$100) (see Figure S3), indicating shear-driven mixing likely due to internal wave breaking.

3.3 Turbulent Drivers of Water Masses Transformation

The OMP analysis assesses the contributions of LCR's and Gulf's waters in each glider sample, revealing the significance of the LCR's periphery in the water mass transformation (Fig. 2i). Layering consists in a stacking of thin layers of salty SUW alternating with thin layers of GCW. This process, driven by mesoscale azimuthal perturbations, reduces the vertical scale of thermohaline intrusions ($\sim$15-80 m) (Meunier et al., 2019). At these scales, DDC can trigger overturning even at low buoyancy Reynolds numbers (see Figure S3), enhancing the turbulent fluxes (Fig.2d, e, f), and leading to the forma-

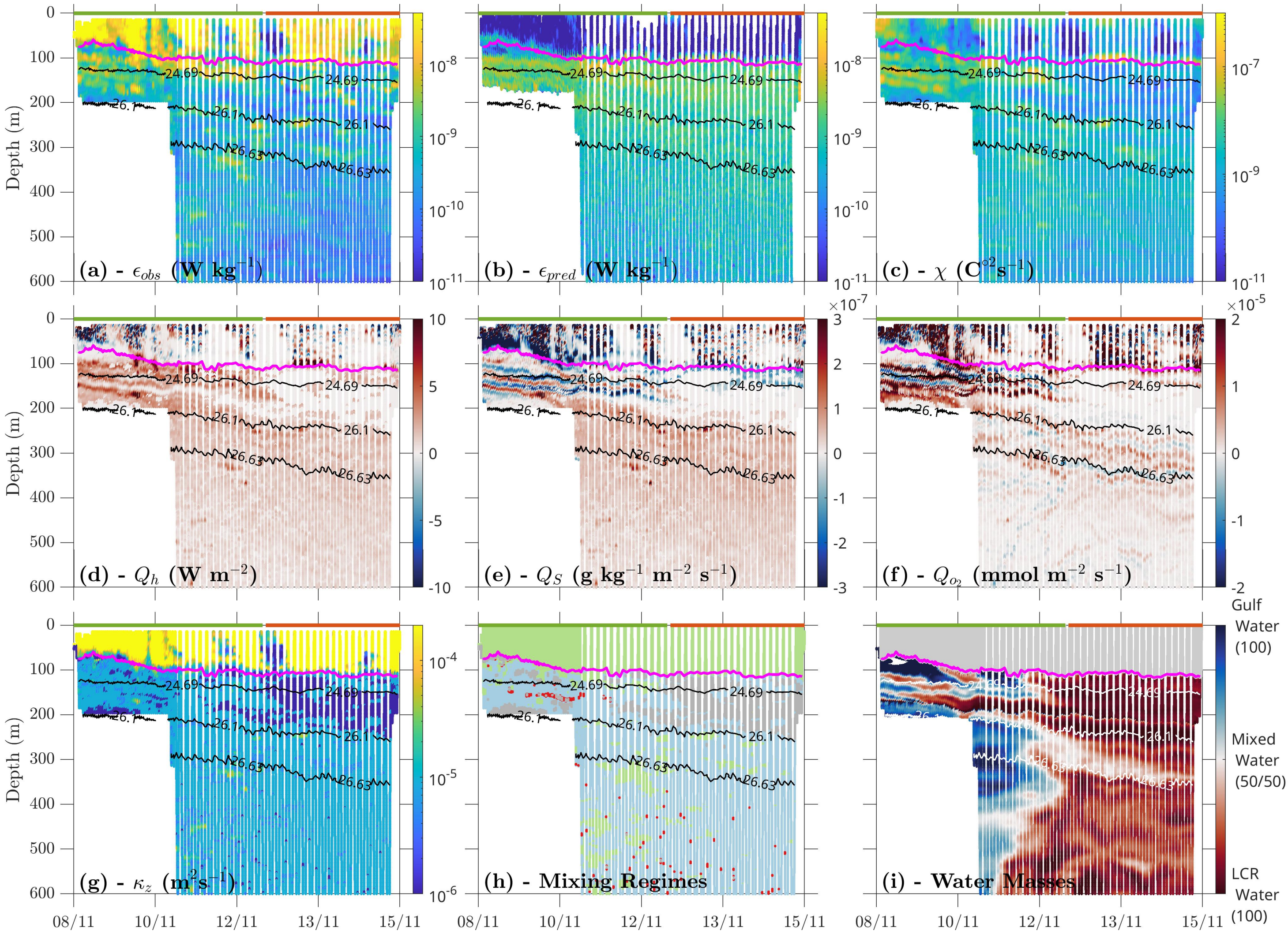

Figure 2. Glider azimuthal section showing: (a) the dissipation rates of turbulent kinetic energy from microstucture; (b) same as (a) but parameterized from Middleton et al. (2021)'s method; (c) the rate of destruction of temperature variance; (d, e, f) vertical turbulent fluxes of heat, salt, and oxygen, respectively; (g) eddy diffusivity; (h) mixing regimes based on the buoyancy Reynolds number and the density ratio, with shear-driven mixing in green, double-convection in red, salt-finger in blue, and areas of no mixing in grey; and (i) water mass transformation expressed as percentages of LCR's and Gulf's waters. The green and orange lines at the top of each panel denote the eddy's periphery and center, respectively. Additionally, the magenta and black lines represent the mixed-layer depth and isopycnes, respectively.

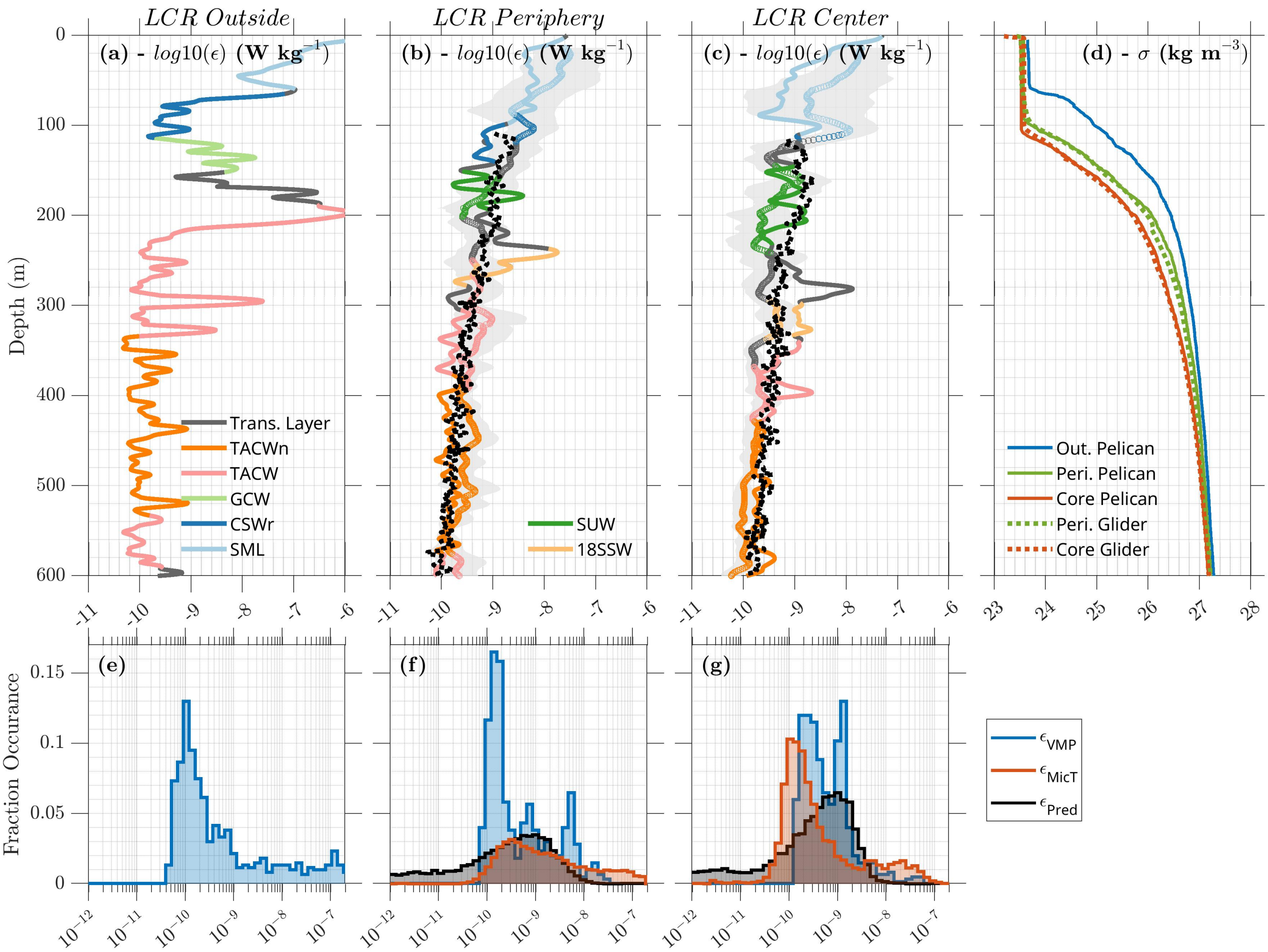

Figure 3. (a, b, c) Averaged profiles of turbulent dissipation rates: solid lines for VMP measurements collected from RV Pelican, colored dots for glider microstructure observations, and black dots for parameterized estimates from double-diffusive convection (Middleton et al., 2021), across eddy periphery and center. Colors correspond to the water masses characterized in Fig. 1h. (d) Profiles of density anomaly sorted by eddy location (Out. for outside, Peri. for periphery) and compared between the different platforms (RV Pelican vs. glider). (e, f, g) Log-histograms comparing predicted dissipation rates (ε_{Pred}) with observed rates from microstructure (ε_{MicT}) and VMP (ε_{VMP}), covering areas outside the eddy (e), its periphery (f), and center (g), respectively.

tion of well-mixed transition layers (Fig.2i). Additional well-mixed regions are observed: (i) between the LCR's periphery and core below 200 m, and (ii) beneath the SUW core in the eddy's center ($\sim$300 m) where oxygen-rich 18SSW water is found (Fig. 1h). Both mixed water columns closely match with increased ε (Fig. 2a), which is induced by a mixture of shear-driven and DDC mixing (Fig. 2h).

Ultimately, watermass properties are irreversibly mixed at the dissipative scale. Fig. 4 illustrates the contribution of different turbulent processes in vertical turbulent fluxes of heat, salt, and oxygen, across the isopycnal layers displayed in Fig. 1b. Vertical fluxes are normalized according to the thickness of each isopycnal layer, allowing for comparison between layers. Although DDC conditions are prevalent in 70% of cases (Fig. 2h), shear-driven mixing is the major contributor to dissipation within the LCR, accounting in average for 78% of observed ε (Fig. 4a). Additionally, 85% of this mixing is localized in the eddy's periphery, highlighting its critical role in transforming water masses, as shown in Fig. 2i. While shear-driven mixing dominates in terms of dissipation, DDC accounts in average for $\sim$70% of the vertical turbulent fluxes of heat, salt, and oxygen (Fig. 4), because of its ability to convert potential energy into TKE, e.g. $\Gamma = -1$, indicating that the effective diffusivity is underestimated by $\Gamma = 0.2$.

The ability of DDC to force turbulence at low Re_b can be assessed in the LCR by comparing the magnitudes and patterns of the observed average dissipation rate, to the predicted dissipation rate from double-diffusive convection parameterized following Middleton et al. (2021) (Fig. 3b, c, black dots). Histograms of the estimated and observed dissipation rates from microstructure show similar distribution in the eddy's periphery (Fig. 3f), and well-reproduce the enhanced ε induced by the layering (Fig. 2b). However, in the eddy center, results show that the parameterized dissipation rate due to DDC is overestimated compared to observations (Fig. 3g). The DDC parameterization assumes a k^{-1} slope for the variance spectrum of spice, which is likely an overestimate in this region due to the weak stirring, leading to the overestimation of mixing within the SUW core (Fig. 2b), as in Fine et al. (2022). Whilst the density ratio Fig. 2h is a mixture of doubly stable, salt fingering favourable and diffusive convection favourable, the buoyancy Reynolds number is skewed to the left, i.e.,$<$10 (see Figure S3), suggesting that in most cases, stratification suppresses shear-production. Vertical fluxes are therefore largely driven by DDC triggering turbulence in the LCR.

3.4 Vertical Turbulent Fluxes

The vertical fluxes of heat, salt, and oxygen between the isopycnals layers, based on the water mass distribution in the LCR are shown in Figure 4. Our analysis reveals that vertical fluxes of heat and oxygen are predominantly downward (positive), except in the deeper region where oxygen fluxes are upward (negative, Fig. 4b, d). Below the 24.69 kg m^{-3} isopycnal, the water column warms and gains oxygen, as indicated by the positive net fluxes (Fig. 4b, d). In contrast, the layer just below the MLD shows the opposite, with cooling (-412 W m^{-1}) and deoxygenation (-7.9$\times$10^{-4} mmol m^{-1} s^{-1}) due to its interaction with surface forcings. Vertical salt fluxes exhibit a more complex pattern with a divergence around the 24.69 to 26.1 kg m^{-3} isopycnal, where thermohaline intrusions are found (Fig. 2a). The layer above has a net upward flux, while the layer below has a net downward flux (Fig. 4c). Thermohaline intrusions lead to a net downward salt flux of -0.06 10^{-6} g kg^{-1} m^{-1} s^{-1}, where the SUW is found. Therefore, this double-diffusive process contributes to the erosion of the subsurface maximum salinity of the SUW.

Meunier et al. (2020) suggests that lateral mixing at sub-mesoscale scale ($<$25km) is an important process for LCR's heat dispersion. To get an overview of the turbulent fluxes induced by the thermohaline intrusions, we set $K_{DDC}^{sides} = \Gamma\langle\varepsilon\rangle/\langle N^2\rangle$ with $\Gamma = -1$. This forms the basis for computing horizontal diffusivity for heat, $K_{HT} = K_{DDC}^{sides} T_z^2/T_x^2$

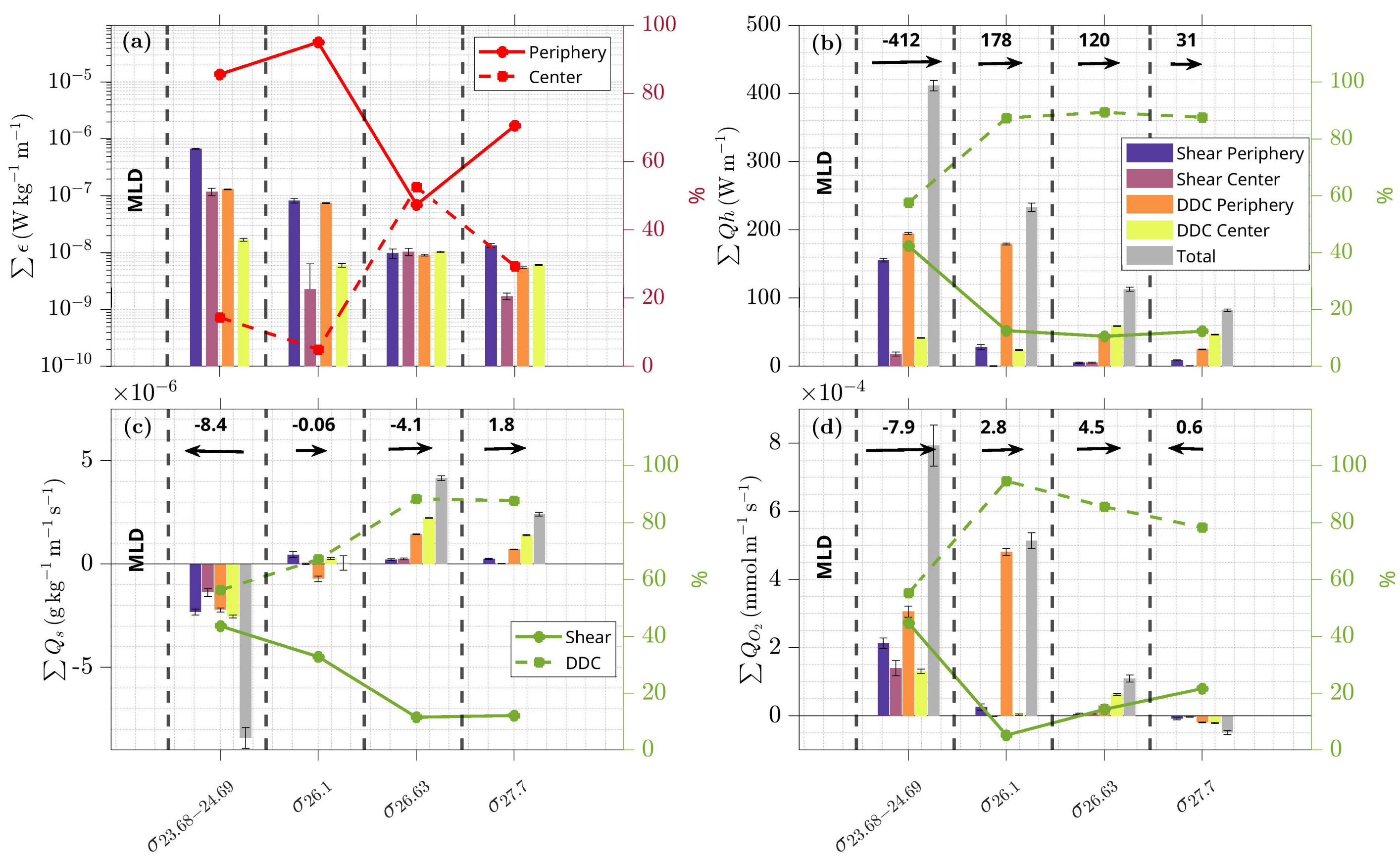

Figure 4. Contribution of (a) dissipation rates and (b, c, d) vertical turbulent fluxes of heat, salt, and oxygen, respectively, segmented by isopycnal layers, based on water mass distribution in the LCR (Fig. 1h). They are categorized by eddy location and mixing nature: shear vs. double-diffusive convection (DDC) (bar color). Relative contributions in each isopycnal layer are shown in % (red and green lines), with net turbulent fluxes changes (+/-) and their directions, downward(upward) fluxes are positive(negative). Vertical fluxes are normalized according to the thickness of each isopycnal layer.

(B. R. Ruddick et al., 2010) and salt, $K_{HS} = K_{DDC}^{sides} S_z^2/S_x^2$ (Hebert et al., 1990). In the thermohaline intrusions, the averaged horizontal heat and salt fluxes are approximately 600 W m^{-2} and 1.8×10^{-5} g kg^{-1} m^{-1} s^{-1}, respectively. These values are two and four orders of magnitude higher than the averaged vertical fluxes, which is consistent with observations in similar finescale structures (Fine et al., 2018; Molodtsov et al., 2020).

4 Summary and Discussion

This observational study provides quantitative estimates of the turbulent processes within an LCR, and their influence on vertical turbulent fluxes and water mass transformation. Our results indicate that shear-driven mixing, does not account for the total heat, salt and oxygen fluxes, and that double-diffusive convection needs to be considered as a key process to explain these turbulent fluxes and water mass transformation.

Through detailed microstructure measurements, we captured the processes driving turbulent mixing. Below the mixed layer, we observed enhanced dissipation rates ($O(10^{-8})$ W kg^{-1}) at the eddy's periphery, beneath its core, and deeper within the eddy. We have shown that DDC can explain the dissipation at the eddy's edges, but not at depth, where it is likely due to internal wave breaking, as observed in various studies (Pallàs-Sanz et al., 2016; Martínez-Marrero et al., 2019; Fernández-Castro et al., 2020). Anticyclonic eddies as LCRs have been shown to induce DDC around their edges in the Arctic (Fine et al., 2018), Mediterranean (Armi et al., 1989; Tokos & Rossby, 1991), Gulf Stream rings (B. R. Ruddick & Bennett, 1985; Schmitt et al., 1986), and the Gulf of Mexico (Meunier et al., 2019; Molodtsov et al., 2020). Additionally, the eddy's periphery emerges as a hotspot responsible for 85% of the total mixing (Fig. 4a), highlighting the need for models to accurately capture this narrow band of few kilometers thick to effectively resolve the processes driving the mesoscale eddy decay.

This study also highlights that submesoscale stirring of spice resulting in DDC is a key mechanism in the route towards transformation of SUW into GCW. We also showed the importance of lateral mixing (few times larger than vertical), associated with thermohaline intrusions, in diffusing the LCR's heat and salt, as suggested in Meunier et al. (2019, 2020). These results challenge the perspective that GCW formation results principally from the vertical mixing of TACW and CSWr (Cervantes-Díaz et al., 2022), suggesting instead that SUW significantly influences GCW formation. Although our observations focus on a single LCR, layering appears to be a recurrent process (Meunier et al., 2019; Molodtsov et al., 2020), and therefore highly relevant for water mass transformation in the GoM.

One important result of this study is the seemingly secondary role played by shear-driven mixing in the eddy's water mass exchanges. Although on average, shear mixing corresponds to $\sim$80% of the total dissipation, the latter accounts for only a third of vertical fluxes within the eddy (Fig. 4). This disparity is attributed to the prevalence of DDC conductive conditions ($\sim$70% of occurrence), where all potential energy is converted into TKE, a mechanism contrasting sharply with shear-driven mixing (Laurent & Schmitt, 1999; Inoue et al., 2007). To verify that DDC is sufficiently strong to control water mass exchanges within the LCR, we applied the parameterization of Middleton et al. (2021) to estimate ε due to double-diffusion. While this method underestimated ε in the high shear regions, it reproduced the enhanced ε observed in the region of enhanced submesoscale stirring on the LCR periphery (Fig. 2b). These findings show that the submesoscale stirring of compensated thermohaline variance (spice) along isopycnals plays an essential role in water mass transformation. Using the classical Osborn (1980) model, with a $\Gamma = 0.2$ suited for shear-driven mixing, leads to a 42% underestimation of vertical turbulent fluxes. However, adjusting $\Gamma = -1$ to capture DDC dynamics (Laurent

& Schmitt, 1999) gives significantly larger rates of vertical turbulent fluxes, hence water mass transformation.

We have shown that double-diffusive convection, favoured by submesoscale stirring, is potentially important in water mass transformation in the Gulf of Mexico. However, the effect of DDC on water mass transformation has not been quantified on a global scale. Given that LCRs are the principal source of water mass variability in the Gulf of Mexico (Portela et al., 2018), an ongoing study is employing both internal-wave (Whalen et al., 2015) and double-diffusive (Middleton et al., 2021) parameterizations to estimate ε across all LCRs identified by the 30 GMOG glider missions since 2016. This effort will aim at enhancing our understanding of warm-core rings' role in tracer transport and diffusion at the basin scale.

5 Open Research

The processed data used in this article needed to understand, evaluate, and build upon the reported research are available in the repository of the Group of Monitoring the Ocean (GMOG). The database is called TurbulentPBE and can accessed using the link `https://gliders.cicese.mx/databases/TurbulentPBE`. Will be required to disclose (i) name, (ii) last name, (iii) e-mail address, (iv) name of the institution, and (v) specify how the TurbulentPBE will be used. GMOG-CICESE will authorize the access and will email to the user a username and password to download the TurbulentPBE database. Anonymous reviewers have granted access to the data, credentials are not required. The TurbulentPBE database can be licensed for non-commerical use, and it is prohibited to share it with third parties, as well as to profit or sell products derived from it. The scripts for microstructure processing are from the MATLAB toolbox (`https://github.com/bscheife/turbulence_temperature`) developed by Scheifele et al. (2018).

Acknowledgments
This work and the postdoctoral fellowship of the corresponding author were supported by the project "Phytoplankton Blooms in a Loop Current Eddy" (FORDECIT-PRONACES/1327709/2020) from Consejo Nacional de Humanidades, Ciencias y Tecnologías de México (CONAHCyT). We acknowledge the contribution of all the staff of Grupo de Monitoreo Oceanográfico con Gliders (GMOG) at the Centro de Investigación Científica y de Educación Superior de Ensenada, Baja California (CICESE), specially to Simo Cusí and Adrian Villicaña for piloting underwater gliders, and to Johanna Saavedra and Eliot Aranda Gonzalez for data management. We are also grateful to the Dr. Anthony Bosse and the Rockland Scientific team, specially the Dr. Anneke ten Doeschate and Evan Cervelli for their support to process glider-MicroPod data.

References

Armi, L., Hebert, D., Oakey, N., Price, J. F., Richardson, P. L., Rossby, H. T., & Ruddick, B. (1989). Two years in the life of a mediterranean salt lens. *Journal of Physical Oceanography*, *19*(3), 354–370.

Batchelor, G. K. (1959). Small-scale variation of convected quantities like temperature in turbulent fluid part 1. general discussion and the case of small conductivity. *Journal of fluid mechanics*, *5*(1), 113–133.

Bebieva, Y., & Timmermans, M.-L. (2016). An examination of double-diffusive processes in a mesoscale eddy in the arctic ocean. *Journal of Geophysical Research: Oceans*, *121*(1), 457–475.

Bouffard, D., & Boegman, L. (2013). A diapycnal diffusivity model for stratified environmental flows. *Dynamics of Atmospheres and Oceans*, *61*, 14–34.

Brannigan, L. (2016). Intense submesoscale upwelling in anticyclonic eddies. *Geo-*

physical Research Letters, *43*(7), 3360–3369.
Cervantes-Díaz, G. Y., Hernández-Ayón, J. M., Zirino, A., Herzka, S. Z., Camacho-Ibar, V., Norzagaray, O., ... Delgado, J. A. (2022). Understanding upper water mass dynamics in the gulf of mexico by linking physical and biogeochemical features. *Journal of marine systems*, *225*, 103647.
Chaigneau, A., Gizolme, A., & Grados, C. (2008). Mesoscale eddies off peru in altimeter records: Identification algorithms and eddy spatio-temporal patterns. *Progress in Oceanography*, *79*(2-4), 106–119.
Damien, P., Sheinbaum, J., Pasqueron de Fommervault, O., Jouanno, J., Linacre, L., & Duteil, O. (2021). Do loop current eddies stimulate productivity in the gulf of mexico? *Biogeosciences*, *18*(14), 4281–4303.
Fernández-Castro, B., Evans, D. G., Frajka-Williams, E., Vic, C., & Naveira-Garabato, A. C. (2020). Breaking of internal waves and turbulent dissipation in an anticyclonic mode water eddy. *Journal of Physical Oceanography*, *50*(7), 1893 - 1914. Retrieved from `https://journals.ametsoc.org/view/journals/phoc/50/7/jpoD190168.xml` doi: 10.1175/JPO-D-19-0168.1
Fine, E. C., MacKinnon, J. A., Alford, M. H., & Mickett, J. B. (2018). Microstructure observations of turbulent heat fluxes in a warm-core canada basin eddy. *Journal of Physical Oceanography*, *48*(10), 2397–2418.
Fine, E. C., MacKinnon, J. A., Alford, M. H., Middleton, L., Taylor, J., Mickett, J. B., ... Peacock, T. (2022). Double diffusion, shear instabilities, and heat impacts of a pacific summer water intrusion in the beaufort sea. *Journal of Physical Oceanography*, *52*(2), 189–203.
Frajka-Williams, E., Brearley, J. A., Nash, J. D., & Whalen, C. B. (2022). New technological frontiers in ocean mixing. In *Ocean mixing* (pp. 345–361). Elsevier.
Gargett, A. E. (1988). The scaling of turbulence in the presence of stable stratification. *Journal of Geophysical Research: Oceans*, *93*(C5), 5021–5036.
Guthrie, J. D., Fer, I., & Morison, J. H. (2017). Thermohaline staircases in the a mundsen b asin: Possible disruption by shear and mixing. *Journal of Geophysical Research: Oceans*, *122*(10), 7767–7782.
Hamilton, J. M., Lewis, M. R., & Ruddick, B. R. (1989). Vertical fluxes of nitrate associated with salt fingers in the world's oceans. *Journal of Geophysical Research: Oceans*, *94*(C2), 2137–2145.
Hamilton, P., Leben, R., Bower, A., Furey, H., & Pérez-Brunius, P. (2018). Hydrography of the gulf of mexico using autonomous floats. *Journal of Physical Oceanography*, *48*(4), 773–794.
Hebert, D., Oakey, N., & Ruddick, B. (1990). Evolution of a mediterranean salt lens: Scalar properties. *Journal of Physical Oceanography*, *20*(9), 1468–1483.
Herring, H. (2010). *Gulf of mexico hydrographic climatology and method of synthesizing subsurface profiles from the satellite sea surface height anomaly.* Dynalysis of Princeton.
Inoue, R., Yamazaki, H., Wolk, F., Kono, T., & Yoshida, J. (2007). An estimation of buoyancy flux for a mixture of turbulence and double diffusion. *Journal of Physical Oceanography*, *37*(3), 611–624.
Ivey, G., Winters, K., & Koseff, J. (2008). Density stratification, turbulence, but how much mixing? *Annu. Rev. Fluid Mech.*, *40*, 169–184.
Jackson, P. R., & Rehmann, C. R. (2014). Experiments on differential scalar mixing in turbulence in a sheared, stratified flow. *Journal of Physical Oceanography*, *44*(10), 2661–2680.
Jaimes, B., Shay, L. K., & Brewster, J. K. (2016). Observed air-sea interactions in tropical cyclone isaac over loop current mesoscale eddy features. *Dynamics of Atmospheres and Oceans*, *76*, 306–324.
John, E. B., Balaguru, K., Leung, L. R., Foltz, G. R., Hetland, R. D., & Hagos, S. M. (2023). Intensification of hurricane sally (2020) over the mississippi river plume. *Weather and Forecasting*.

Kunze, E. (2003). A review of oceanic salt-fingering theory. *Progress in Oceanography*, *56*(3-4), 399–417.

Laurent, L. S., & Schmitt, R. W. (1999). The contribution of salt fingers to vertical mixing in the north atlantic tracer release experiment. *Journal of Physical Oceanography*, *29*(7), 1404–1424.

Linacre, L., Durazo, R., Camacho-Ibar, V., Selph, K., Lara-Lara, J., Mirabal-Gómez, U., ... Sidón-Ceseña, K. (2019). Picoplankton carbon biomass assessments and distribution of prochlorococcus ecotypes linked to loop current eddies during summer in the southern gulf of mexico. *Journal of Geophysical Research: Oceans*, *124*(11), 8342–8359.

Martínez-Marrero, A., Barceló-Llull, B., Pallàs-Sanz, E., Aguiar-González, B., Estrada-Allis, S. N., Gordo, C., ... Arístegui, J. (2019). Near-inertial wave trapping near the base of an anticyclonic mesoscale eddy under normal atmospheric conditions. *Journal of Geophysical Research: Oceans*, *124*(11), 8455–8467.

McDougall, T. J., & Barker, P. M. (2011). Getting started with teos-10 and the gibbs seawater (gsw) oceanographic toolbox. *Scor/Iapso WG*, *127*(532), 1–28.

Meunier, T., Bower, A., Pérez-Brunius, P., Graef, F., & Mahadevan, A. (2024). The energy decay of warm-core eddies in the gulf of mexico. *Geophysical Research Letters*, *51*(1), e2023GL106246. Retrieved from `https://agupubs.onlinelibrary.wiley.com/doi/abs/10.1029/2023GL106246` (e2023GL106246 2023GL106246) doi: https://doi.org/10.1029/2023GL106246

Meunier, T., Ménesguen, C., Schopp, R., & Le Gentil, S. (2015). Tracer stirring around a meddy: The formation of layering. *Journal of Physical Oceanography*, *45*(2), 407–423.

Meunier, T., Pallás-Sanz, E., Tenreiro, M., Portela, E., Ochoa, J., Ruiz-Angulo, A., & Cusí, S. (2018). The vertical structure of a loop current eddy. *Journal of Geophysical Research: Oceans*, *123*(9), 6070–6090.

Meunier, T., Sanz, E. P., Tenreiro, M., Ochoa, J., Angulo, A. R., & Buckingham, C. (2019). Observations of layering under a warm-core ring in the gulf of mexico. *Journal of Physical Oceanography*, *49*(12), 3145–3162.

Meunier, T., Sheinbaum, J., Pallàs-Sanz, E., Tenreiro, M., Ochoa, J., Ruiz-Angulo, A., ... de Marez, C. (2020). Heat content anomaly and decay of warm-core rings: The case of the gulf of mexico. *Geophysical Research Letters*, *47*(3), e2019GL085600.

Middleton, L., Fine, E., MacKinnon, J., Alford, M., & Taylor, J. (2021). Estimating dissipation rates associated with double diffusion. *Geophysical Research Letters*, *48*(15), e2021GL092779.

Molodtsov, S., Anis, A., Amon, R., & Perez-Brunius, P. (2020). Turbulent mixing in a loop current eddy from glider-based microstructure observations. *Geophysical Research Letters*, *47*(14), e2020GL088033.

Monterey, G. I., & Levitus, S. (1997). Seasonal variability of mixed layer depth for the world ocean.

Osborn, T. R. (1980). Estimates of the local rate of vertical diffusion from dissipation measurements. *Journal of physical oceanography*, *10*(1), 83–89.

Osborn, T. R., & Cox, C. S. (1972). Oceanic fine structure. *Geophysical Fluid Dynamics*, *3*(4), 321–345.

Oyabu, R., Yasuda, I., & Sasaki, Y. (2023). Large-scale distribution and variations of active salt-finger double-diffusion in the western north pacific. *Journal of Physical Oceanography*, *53*(8), 2013–2027.

Pallàs-Sanz, E., Candela, J., Sheinbaum, J., & Ochoa, J. (2016). Mooring observations of the near-inertial wave wake of hurricane ida (2009). *Dynamics of Atmospheres and Oceans*, *76*, 325–344.

Pérez, J., Pallàs-Sanz, E., Tenreiro, M., Meunier, T., Jouanno, J., & Ruiz-Angulo, A. (2022). Overturning instabilities across a warm core ring from glider observations. *Journal of Geophysical Research: Oceans*, *127*(4), e2021JC017527.

Peterson, A. K., & Fer, I. (2014). Dissipation measurements using temperature microstructure from an underwater glider. *Methods in Oceanography*, *10*, 44–69.

Pollard, R. T., Rhines, P. B., & Thompson, R. O. (1973). The deepening of the wind-mixed layer. *Geophysical Fluid Dynamics*, *4*(4), 381–404.

Portela, E., Tenreiro, M., Pallàs-Sanz, E., Meunier, T., Ruiz-Angulo, A., Sosa-Gutiérrez, R., & Cusí, S. (2018). Hydrography of the central and western gulf of mexico. *Journal of Geophysical Research: Oceans*, *123*(8), 5134–5149.

Ruddick, B., Anis, A., & Thompson, K. (2000). Maximum likelihood spectral fitting: The batchelor spectrum. *Journal of Atmospheric and Oceanic Technology*, *17*(11), 1541–1555.

Ruddick, B., & Richards, K. (2003). Oceanic thermohaline intrusions: Observations. *Progress in Oceanography*, *56*(3-4), 499–527.

Ruddick, B. R., & Bennett, A. S. (1985). Fine structure and mixing at the edge of a warm core ring. *Journal of Geophysical Research: Oceans*, *90*(C5), 8943–8951.

Ruddick, B. R., Oakey, N. S., & Hebert, D. (2010). Measuring lateral heat flux across a thermohaline front: A model and observational test. *Journal of Marine Research*, *68*(3-4), 523–539.

Sanchez-Rios, A., Shearman, R. K., Lee, C. M., Simmons, H. L., St. Laurent, L., Lucas, A. J., … Jan, S. (2024). Characterization of mixing at the edge of a kuroshio intrusion into the south china sea: analysis of thermal variance diffusivity measurements. *Journal of Physical Oceanography*.

Scheifele, B., Waterman, S., Merckelbach, L., & Carpenter, J. R. (2018). Measuring the dissipation rate of turbulent kinetic energy in strongly stratified, low-energy environments: A case study from the arctic ocean. *Journal of Geophysical Research: Oceans*, *123*(8), 5459–5480.

Schmitt, R. W. (1994). Double diffusion in oceanography. *Annual review of fluid mechanics*, *26*(1), 255–285.

Schmitt, R. W., Lueck, R. G., & Joyce, T. M. (1986). Fine-and microstructure at the edge of a warm-core ring. *Deep Sea Research Part A. Oceanographic Research Papers*, *33*(11-12), 1665–1689.

Shay, L. K., Goni, G. J., & Black, P. G. (2000). Effects of a warm oceanic feature on hurricane opal. *Monthly Weather Review*, *128*(5), 1366–1383.

Shcherbina, A. Y., Gregg, M. C., Alford, M. H., & Harcourt, R. R. (2009). Characterizing thermohaline intrusions in the north pacific subtropical frontal zone. *Journal of Physical Oceanography*, *39*(11), 2735–2756.

Shibley, N., & Timmermans, M.-L. (2019). The formation of double-diffusive layers in a weakly turbulent environment. *Journal of Geophysical Research: Oceans*, *124*(3), 1445–1458.

Shih, L. H., Koseff, J. R., Ivey, G. N., & Ferziger, J. H. (2005). Parameterization of turbulent fluxes and scales using homogeneous sheared stably stratified turbulence simulations. *Journal of Fluid Mechanics*, *525*, 193–214.

Sosa-Gutiérrez, R., Pallàs-Sanz, E., Jouanno, J., Chaigneau, A., Candela, J., & Tenreiro, M. (2020). Erosion of the subsurface salinity maximum of the loop current eddies from glider observations and a numerical model. *Journal of Geophysical Research: Oceans*, *125*(7), e2019JC015397.

Stillinger, D., Helland, K., & Van Atta, C. (1983). Experiments on the transition of homogeneous turbulence to internal waves in a stratified fluid. *Journal of Fluid Mechanics*, *131*, 91–122.

Thirion, G., Birol, F., & Jouanno, J. (2024). Loop current eddies as a possible cause of the rapid sea level rise in the gulf of mexico. *Journal of Geophysical Research: Oceans*, *129*(3), e2023JC019764.

Tokos, K. S., & Rossby, T. (1991). Kinematics and dynamics of a mediterranean salt lens. *Journal of Physical Oceanography*, *21*(6), 879–892.

Tomczak, M. (1999). Some historical, theoretical and applied aspects of quantitative water mass analysis. *Journal of Marine Research*, *57*(2), 275–303.
Tomczak, M., & Large, D. G. (1989). Optimum multiparameter analysis of mixing in the thermocline of the eastern indian ocean. *Journal of Geophysical Research: Oceans*, *94*(C11), 16141–16149.
Tomczak Jr, M. (1981). A multi-parameter extension of temperature/salinity diagram techniques for the analysis of non-isopycnal mixing. *Progress in Oceanography*, *10*(3), 147–171.
Vidal, V. M., Vidal, F. V., Hernández, A. F., Meza, E., & Zambrano, L. (1994). Winter water mass distributions in the western gulf of mexico affected by a colliding anticyclonic ring. *Journal of Oceanography*, *50*, 559–588.
Washburn, L., & Käse, R. H. (1987). Double diffusion and the distribution of the density ratio in the mediterranean waterfront southeast of the azores. *Journal of physical oceanography*, *17*(1), 12–25.
Whalen, C. B., MacKinnon, J. A., Talley, L. D., & Waterhouse, A. F. (2015). Estimating the mean diapycnal mixing using a finescale strain parameterization. *Journal of Physical Oceanography*, *45*(4), 1174–1188.
Wu, L., Rutgersson, A., & Sahlée, E. (2015). Upper-ocean mixing due to surface gravity waves. *Journal of Geophysical Research: Oceans*, *120*(12), 8210–8228.
Yang, Y., Verzicco, R., & Lohse, D. (2016). From convection rolls to finger convection in double-diffusive turbulence. *Proceedings of the National Academy of Sciences*, *113*(1), 69–73.

Supporting Information for "Distribution, Mixing, and Transformation of a Loop Current Ring Waters: The Case of Gulf of Mexico"

Mathieu Gentil[1], Enric Pallàs-Sanz[1], Leo Middleton[2], Angel Ruiz-Angulo[3], Thomas Meunier[1,2,4], Giovanni Durante[1], Miguel Tenreiro[1], Sheila N. Allis Estrada[1], Julio Sheinbaum[1]

[1]Center for Scientific Research and Higher Education at Ensenada, Ensenada, Mexico
[2]Woods Hole Oceanographic Institution, Woods Hole, MA, USA
[3]Institute of Earth Sciences, University of Iceland, 102 Reykjavik, Iceland
[4]Laboratoire d'Océanographie Physique et Spatiale (LOPS), University of Brest, CNRS, IRD, Ifremer, IUEM, France

Contents of this file

Description

- Text S1: We use the parameterization developed by Middleton et al. (2021) to estimate the dissipation rate associated with double-diffusive convection. This parameterization works by estimating the turbulent buoyancy flux $\langle wb \rangle$, and assuming it is in balance with the dissipation rate ε. They estimate the turbulent buoyancy flux by using an assumption of balance in the variance equation for buoyancy, following Osborn and Cox (1972). In other words, they assume that the available potential energy within the small scale turbulence is in a quasi-steady state, so the primary balance is between the diapycnal buoyancy flux:

$$\Phi_d = \left\langle \frac{(\kappa_T + \kappa_S)}{2b_z^*}|\nabla b|^2 + \frac{(\kappa_T - \kappa_S)}{2b_z^*}\nabla b \cdot \nabla s_p \right\rangle, \quad (1)$$

  and the turbulent buoyancy flux $\langle w'b' \rangle$, averaged over the space between observations. Here b_z^* is the adiabatically resorted buoyancy profile, and s_p denotes the 'spice', which is defined using a linear equation of state as $s_p = g\alpha T + g\beta S$ for the purposes of the parameterization.
  The diapycnal buoyancy flux Φ_d is estimated from observations by assuming that spice has a steeper spectral slope for its power spectrum than does buoyancy. So the buoyancy gradient is estimated using observations of N^2, and we assume a spectral slope of k^{-1} for the power spectrum of spice on sub-observational scales. The magnitude of the spice gradient at the overturning scale $|\nabla s_p|$ is estimated by fitting a power spectrum between each pair of observations using a two-point correlation along an isopycnal. The assumed slope of the spectrum can be altered to account for lesser degrees of stirring of spice. The full account of the iterative method used to calculate Φ_d can be found in Middleton et al. (2021). This method assumes double-diffusive convection is present, as it relies on the second term of Φ_d which is purely double diffusive (if the molecular diffusivities κ_T and κ_S are equal, this term dissapears). The parameterization also assumes an anti-correlation between ∇b and ∇s_p on overturning scales, which amounts to an assumption that double-diffusive convection is present.

- Figure S1 shows the parameters used for the optimal multiparameter analysis: conservative temperature (θ), absolute salinity (S_A) , dissolved oxygen (O_2), and potential vorticity (P_V). The source water types are defined as (quasi) continuous lines in the parameter space considering the most characteristic values of the water masses involved. We used the CTD cast data to find the characteristic parameter values in the entire profile from the Loop Current Ring (LCR) center (red line) and those taken outside of the LCR (blue line), based on the range defined in Portela et al. (2018). We focused on complete profiles because we aim to examine the transitional waters between the pure LCR or Caribbean waters and the mature forms of the Gulf waters, such as Gulf Common Water, as glider samples are collected near the LCR boundary.

- Figure S2 describes the distribution of temperature staircases in the water column. Double-diffusive convection (DDC) may be characterized by a Turner Angle of -45/-90 rad^{-1} and 45/90 rad^{-1} for the diffusive convection (DC) and salt fingering (SF) conditions, respectively. The Turner angle shows two areas susceptible to DDC conditions, (i) the thermohaline intrusions (blue square), and (ii) salt-fingers favourable conditions (red square). In the blue square, spice anomalies are greater than density anomalies (panel c), in average by a factor 2, which is a typical pattern of thermohaline intrusions or layering (Meunier et al., 2019). These structures present thermohaline staircases up to 20 m of vertical length (panel d), which are of similar size than the spice anomalies. A second area, below 200 m depth, shows SF conductive conditions (red square in panel b). As shown in panel e, spice anomalies are smaller or compensated by density anomalies. High-resolution temperature profiles from the thermistor reveal indistinct thermohaline staircases (panel f).

- Figure S3 shows the buoyancy Reynolds number (R_{eb}) estimated from the vertical microstructure profiler (VMP), the glider-microstructure and the DDC parameterization from Middleton et al. (2021). This number is calculated as the ratio of the dissipation rates, which promotes vertical overturns, to the potential energy of stratification, which suppresses these overturns. A threshold for the buoyancy Reynolds number is ∼10; values below this threshold generally indicate that diapycnal turbulent mixing is suppressed (Stillinger et al., 1983; Shih et al., 2005; Ivey et al., 2008; Bouffard & Boegman, 2013). A large number of estimates, ranging from ∼63% to 77%, occurred under conditions where Re_b <10, regardless of the measurement platform. This suggests that stratification effectively suppresses shear-productions in most cases, indicating that turbulent fluxes are predominantly driven by DDC. However, a bimodal distribution is observed for VMP and glider estimates, with a peak in the turbulent regime Re_b >10, mainly induced by intense mixing in the surface mixed layer. This bimodal distribution is not captured by $Re_{b_{Pred}}$, because the double-diffussive convection parameterization fails to represent the shear-driving or internal waves breaking mixing.

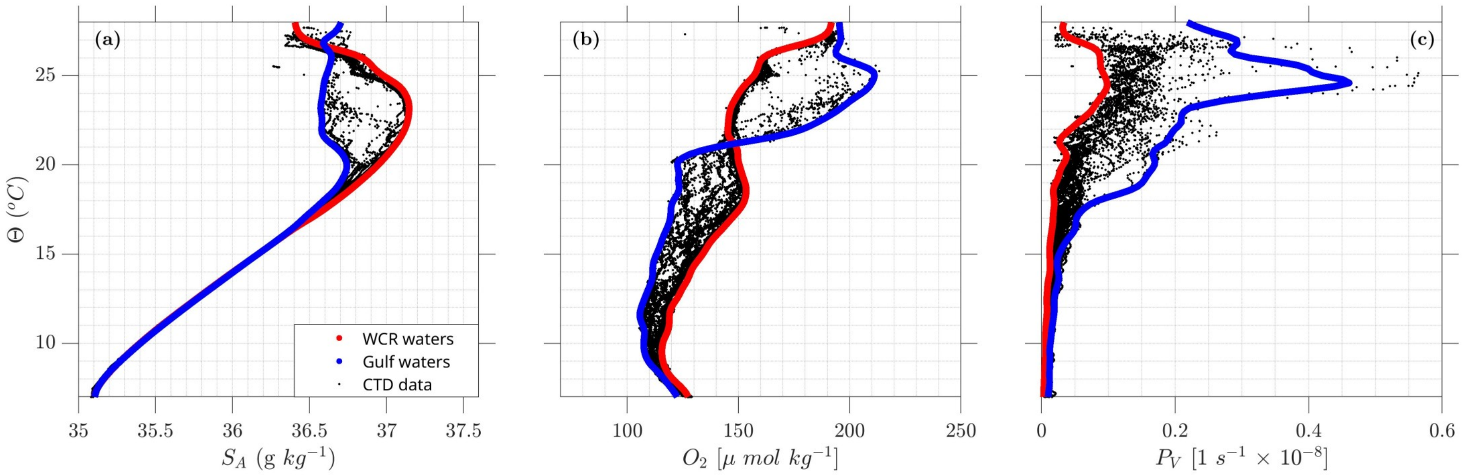

Figure S1. Source water types definition in the parameter space. The blue lines are for the Gulf waters and the red ones are for LCR waters. Black dots represent the CTD data used to separate the profiles within the eddy and outer profiles. (a) θ-S_A, (b) θ-O_2, and (c) θ-P_V diagrams.

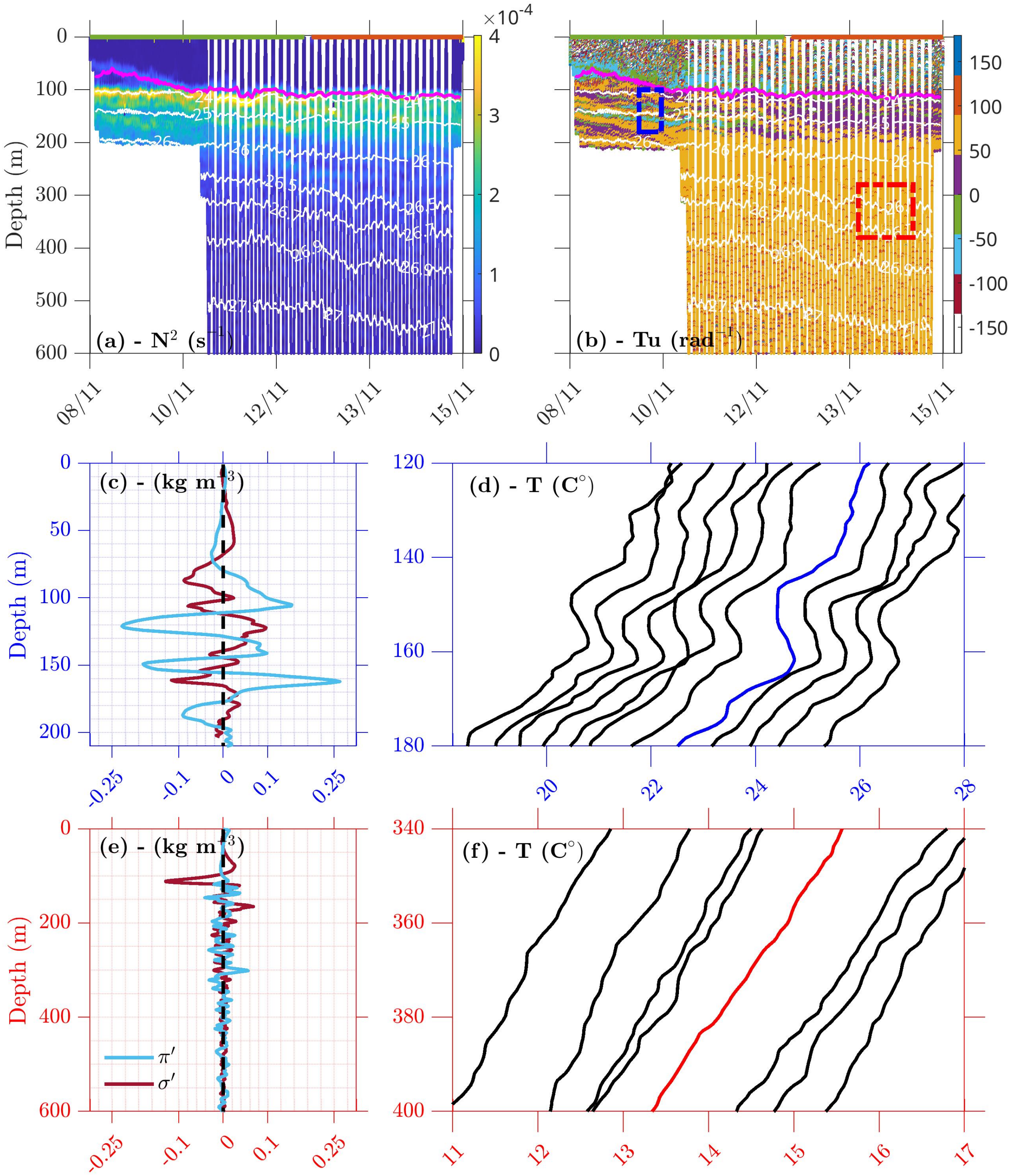

Figure S2. Glider section of (a) Brunt-Väisälä frequency and (b) Turner angle, where regions that are susceptible to double-diffusive convection are indicated by values of -45/-90 rad^{-1} (double-convection: light blue), and 45/90 rad^{-1} (salt-finger: yellow). Regions of thermohaline intrusions (blue square) and salt finger conditions (red square) were highlighted. (c) and (e) are one of the spice (blue) and density (red) anomaly profile from the blue and red square of (b) respectively. (d) and (f) are a selection of temperature profiles (presented as relative temperature, shifted by and offset of 0.5°C) recorded by the FP07 fast thermistor in the blue and red square of (b), respectively. The blue and red profiles are those represented in (c) and (e), respectively.

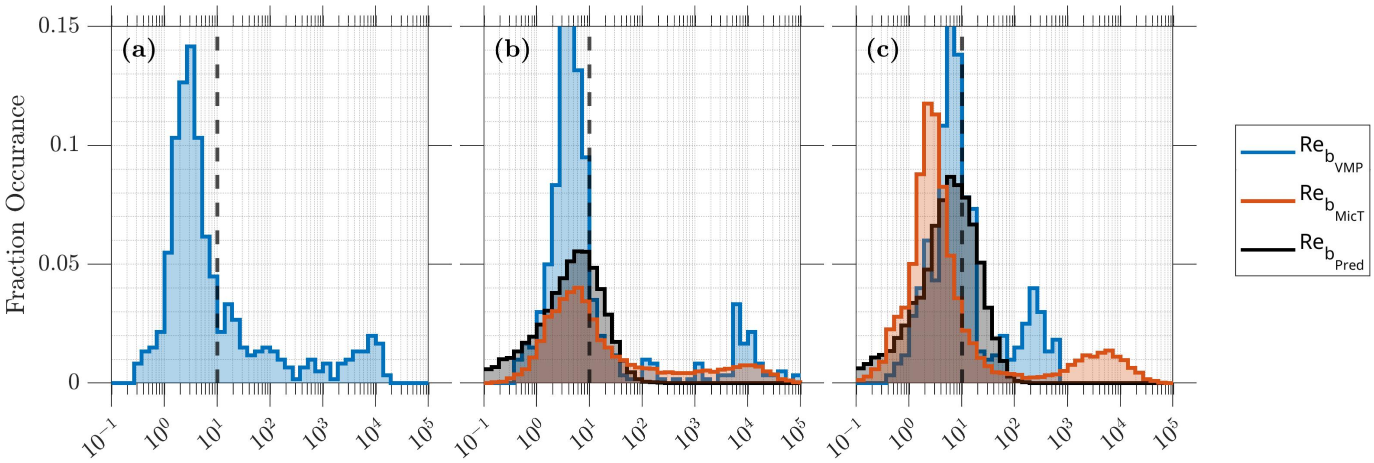

Figure S3. (a, b, c) Log-histograms comparing predicted buoyancy Reynolds number ($Re_{b_{Pred}}$) from double-diffusive convection parameterization (Middleton et al., 2021), with estimates from microstructure ($Re_{b_{MicT}}$) and VMP ($Re_{b_{VMP}}$), covering areas outside the eddy (a), its periphery (b), and center (c), respectively.

References

Bouffard, D., & Boegman, L. (2013). A diapycnal diffusivity model for stratified environmental flows. *Dynamics of Atmospheres and Oceans*, *61*, 14–34.

Ivey, G., Winters, K., & Koseff, J. (2008). Density stratification, turbulence, but how much mixing? *Annu. Rev. Fluid Mech.*, *40*, 169–184.

Meunier, T., Sanz, E. P., Tenreiro, M., Ochoa, J., Angulo, A. R., & Buckingham, C. (2019). Observations of layering under a warm-core ring in the gulf of mexico. *Journal of Physical Oceanography*, *49*(12), 3145–3162.

Middleton, L., Fine, E., MacKinnon, J., Alford, M., & Taylor, J. (2021). Estimating dissipation rates associated with double diffusion. *Geophysical Research Letters*, *48*(15), e2021GL092779.

Osborn, T. R., & Cox, C. S. (1972). Oceanic fine structure. *Geophysical Fluid Dynamics*, *3*(4), 321–345.

Portela, E., Tenreiro, M., Pallàs-Sanz, E., Meunier, T., Ruiz-Angulo, A., Sosa-Gutiérrez, R., & Cusí, S. (2018). Hydrography of the central and western gulf of mexico. *Journal of Geophysical Research: Oceans*, *123*(8), 5134–5149.

Shih, L. H., Koseff, J. R., Ivey, G. N., & Ferziger, J. H. (2005). Parameterization of turbulent fluxes and scales using homogeneous sheared stably stratified turbulence simulations. *Journal of Fluid Mechanics*, *525*, 193–214.

Stillinger, D., Helland, K., & Van Atta, C. (1983). Experiments on the transition of homogeneous turbulence to internal waves in a stratified fluid. *Journal of Fluid Mechanics*, *131*, 91–122.